

國立交通大學

應用數學系

博士論文

多電子系統於半導體量子點上之數值研究



Numerical Studies of the Many-Electron System

in Semiconductor Quantum Dots

研究生：陳人豪

指導教授：劉晉良 教授

中華民國九十六年五月

多電子系統於半導體量子點上之數值研究

Numerical Studies of the Many-Electron System
in Semiconductor Quantum Dots

研究生：陳人豪

Student : Jen-Hao Chen

指導教授：劉晉良

Advisor : Jinn-Liang Liu

國立交通大學

應用數學系



Submitted to Department of Applied Mathematics
College of Science

National Chiao Tung University

in partial Fulfillment of the Requirements

for the Degree of

Doctor of Philosophy

in

Applied Mathematics

May 2007

Hsinchu, Taiwan, Republic of China

中華民國九十六年五月

多電子系統於半導體量子點上之數值研究

學生：陳人豪

指導教授：劉晉良 教授

國立交通大學應用數學系博士班

摘 要

本論文分為兩部份，在第一個部分，我們利用電流自旋密度泛函理論，對於三個垂直排列成一行的半導體量子點提出了一個理論模型，並利用一些數值方法來探究。此量子點分子模型是由三度空間中的硬牆侷限位能以及外部磁場所組成，由於非拋物能帶有效質量的採用，多電子的 Hamiltonian 在有限差分法下，會導出一個三次特徵值問題。而我們利用自恰法來獲得在量子點分子中六個電子的 Kohn-Sham 軌域及能量，其中薛丁格方程與卜易松方程分別由 Jacobi-Davidson 方法與 GMRES 所解出，從數值結果中，我們可以得知原本在無磁場下，六個電子都位於中間的量子點，但在施加適當之磁場後，每一個量子點都有兩個電子，Förster-Dexter 共振能量轉換效應也許因此可由兩個量子點分子所形成，並提供

量子計算中費米量子位元一個新的設計概念。

在第二個部份，我們對半導體量子點中多電子的 Hamiltonian 之精確對角化提出了一個新的方法，由於我們的量子點模型是由三度空間的硬牆侷限位能以及非拋物能帶有效質量所組成，因此一些解析基底，例如拉格爾多項式，在此類模型中是無法使用。在本方法中，我們利用單電子波函數所組成的 Slater 行列式基底來建構多電子系統之波函數，其中單電子 Hamiltonian 中使用了一個與能量及位置相關的有效質量，並加入了適當的邊界條件，利用有限差分法，同樣也得到了三個三次特徵值問題，並且亦透過 Jacobi-Davidson 方法來解，而多電子 Hamiltonian 中的庫倫矩陣元素則是透過解卜易松問題來獲得，我們的數值結果呈現只須少許的單電子基底便可得到一個良好的收斂狀態。

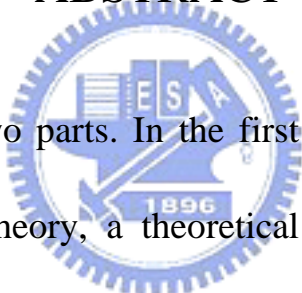
Numerical Studies of the Many-Electron System in Semiconductor Quantum Dots

Student : Jen-Hao Chen

Advisor : Dr. Jinn-Liang Liu

Department of Applied Mathematics
National Chiao Tung University

ABSTRACT

The logo of National Chiao Tung University is a circular emblem with a blue border. Inside the circle, there are stylized Chinese characters and the year '1896'. The letters 'E', 'S', and 'A' are also visible within the design.

This thesis consists of two parts. In the first part, based on the current spin density functional theory, a theoretical model of three vertically aligned semiconductor quantum dots is proposed and numerically studied.

This quantum dot molecule (QDM) model is treated with realistic hard-wall confinement potential and external magnetic field in three-dimensional setting. Using the effective-mass approximation with band nonparabolicity, the many-body Hamiltonian results in a cubic eigenvalue problem from a finite difference discretization. A self-consistent algorithm for solving the Schrödinger-Poisson system by using the Jacobi-Davidson method and GMRES is given to illustrate

the Kohn-Sham orbitals and energies of six electrons in the molecule with some magnetic fields. It is shown that the six electrons residing in the central dot at zero magnetic field can be changed to such that each dot contains two electrons with some feasible magnetic field. The Förster-Dexter resonant energy transfer may therefore be generated by two individual QDMs. This may motivate a new paradigm of Fermionic qubits for quantum computing in solid-state systems.

In the second part, we propose a new approach to the exact diagonalization of many-electron Hamiltonian in semiconductor quantum dot (QD) structures. The QD model is based on realistic 3D finite hard-wall confinement potential and nonparabolic effective mass approximation that render analytical basis functions such as Laguerre polynomials inaccessible for the numerical treatment of this kind of models. In this approach, the many-electron wave function is expanded in a basis of Slater determinants constructed from numerical wave functions of the single-electron Hamiltonian with the energy and position dependent electron effective mass approximation and suitable boundary conditions which result in a cubic eigenvalue problem from a finite difference

discretization. The nonlinear eigenvalue problem is also solved by using the Jacobi-Davidson method. The Coulomb matrix elements in the many-electron Hamiltonian are obtained by solving Poisson's problems via GMRES. Numerical results reveal that a good convergence can be achieved by means of a few single-electron basis states.



致 謝

本論文得以完成，首先要感謝恩師 劉晉良教授多年來的悉心指導與策勵支持，老師除了卓越的專業知識外，其嚴謹的治學態度與追求新知的熱誠，更是學生在研究旅程上永遠的標竿。師恩浩瀚，學生必永記於心。

論文口試期間，承蒙林文偉教授、賴明治教授、葉立明教授、陳宜良教授、簡澄陞教授與呂宗澤教授等諸位審查委員，對本論文提供許多寶貴的意見與指正，使論文更臻完善，學生特此僅致誠摯的謝意。此外，亦感謝系上的老師、助理、同學們曾經給予的協助與鼓勵。

感謝父親陳鴻基先生、母親黃淑英女士的養育之恩與用心栽培，讓我能無後顧之憂的完成學業。要特別感謝是太太孔驪，一路任勞任怨的付出與扶持，給予莫大的鼓勵讓我得以倘佯在研究的旅程中。感謝妹妹幸宜與妹婿稟鎔的關心及替遠在外地求學的我照顧父母。也要感謝岳父劉家霖先生與岳母楊鳳霞女士願意將您的女兒嫁給尚未立業的我。最後，僅以此論文獻給曾經幫助、關心過我的人，並再一次向恩師劉晉良教授致上最深的謝意。

Contents

Abstract (in Chinese)	i
Abstract (in English)	iii
Acknowledgements (in Chinese)	vi
Contents	vii
List of Figures	ix

I A Model for Semiconductor Quantum Dot Molecule Based on the Current Spin Density Functional Theory

1 Introduction	1
2 The Current Spin Density Functional Theory for the Model System	5
3 Numerical Methods and Algorithms for the Model System	12
4 Numerical Results	22
5 Concluding Remarks	28

II A Numerical Method for Exact Diagonalization of Semiconductor Quantum Dot Model

6 Introduction	31
7 Single-Electron Model	36
8 Numerical Methods for Single Electron Wave Functions	38
9 Many-Electron Model	41
An Example	43
10 Numerical Methods for Coulomb Matrix Elements	47
11 Numerical Results	52

12 Concluding Remarks	57
13 Conclusions	58
Appendix	61
Bibliography	66



List of Figures

1.1	Three vertically aligned InAs/GaAs quantum dots with cylindrically symmetric domain in real space dimensions in nano meters that are used in numerical implementation. The domain in 2D setting is denoted by Ω with the boundary $\partial\Omega$ consisting of the south (S), east (E), north (N), and west (W) sides.	4
4.1	The effect of the domain size on the first three energies at $B = 0$.	26
4.2	Contour of KS orbitals at $B=0$ (left panel) and $B=15$ (right panel).	27
7.1	A cross section of a disk-shaped <i>InAs</i> quantum dot embedded in the <i>GaAs</i> matrix in real space dimensions in nano meters that are used in numerical implementation.	37
11.1	The effect of the domain size on the ground state energy of two-electron system with the basis size $N_s = 8$	55
11.2	The ground state energies of two- and four-electron QDs as a function of the basis size N_s from 8 to 18.	56

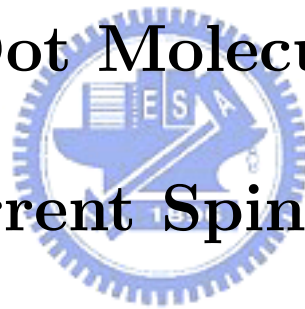
Part I

A Model for Semiconductor

Quantum Dot Molecule Based on

the Current Spin Density

Functional Theory



Chapter 1

Introduction

There is significant interest in quantum information processing based on Fermionic qubits using semiconducting materials [1-10]. One of the proposals in this approach is to exploit electronic excitations of coupled quantum dots (QDs) that form an artificial molecule (QDM) [6] [7] [9] [10]. In particular, an energy selective scheme to manipulating excitonic states of QDM, together with control over the Förster-Dexter resonant energy transfer and biexciton binding energy, can be used to perform quantum computation and to produce controlled exciton quantum entanglement [7] [11]. The resonant Förster-Dexter energy transfer mechanism is also responsible for photosynthetic energy process in antenna complexes, biosystems that harvest sunlight [12]. It has been recently shown that two individual closely spaced fluorescent molecules undergo a strong coherent dipole-dipole coupling can produce entangled states [13]. We propose and numerically investigate here a theoretical model of three vertically aligned InAs/GaAs QDM whose dimensions are commensurable with that of [9] in which a transmission electron micrograph of a QDM sample is illustrated.

Our QDM model consists of one large central dot and two smaller dots situated

above and beneath the central dot whose geometrical dimensions are shown in Fig. 1.1 where the radius, thickness, and separation of each dot are indicated by coordinates. It has been demonstrated in [11] [14] that there exists Förster energy transfer from smaller to larger dots via electrostatic coupling. Our goal for this model system is to investigate the detailed electronic properties of the QDM with $N = 6$ electrons under the effects of an external magnetic field by using the current spin density functional theory (CSDFT) [15] [16].

For the many-body Hamiltonian of our QDM model, we extend the models used in [17-19], which are based on parabolic one-band effective-mass envelope function approximation with either infinite or quadratic confinement potentials, to a more realistic finite confinement potential with band nonparabolicity that leads to an energy-dependent mass in the Hamiltonian for electrons. The nonparabolicity is derived from a projection from the eight-band Kane Hamiltonian into the 2×2 conduction space and hence gives more accurate results as shown in [20-23].

The CSDFT applied to the QDM system with three-dimensionality of the finite confinement and band nonparabolicity poses a very challenging task for the numerical implementation. The energy-dependent mass in the Hamiltonian results in a cubic eigenvalue problem from, e.g., a finite difference discretization. The Jacobi-Davidson (JD) method developed in [24] [25] is extended and incorporated into a self-consistent algorithm for solving the Schrödinger-Poisson system that

implements the CSDFT in real space. We also give a detailed description of the computational algorithm, the Poisson solver, and the approximation methods for the exchange-correlation (xc) energy.

Numerical results on the Kohn-Sham (KS) orbitals and energies of six electrons in the molecule with some magnetic fields are presented in detail. It is shown that the six electrons residing in the central dot at zero magnetic field can be changed to such that each dot contains two electrons with some feasible magnetic field. The Förster energy transfer may therefore be generated by two individual QDMs. This may motivate a new paradigm of Fermionic qubits for quantum computing in solid-state systems, which will be reported in a coming paper.



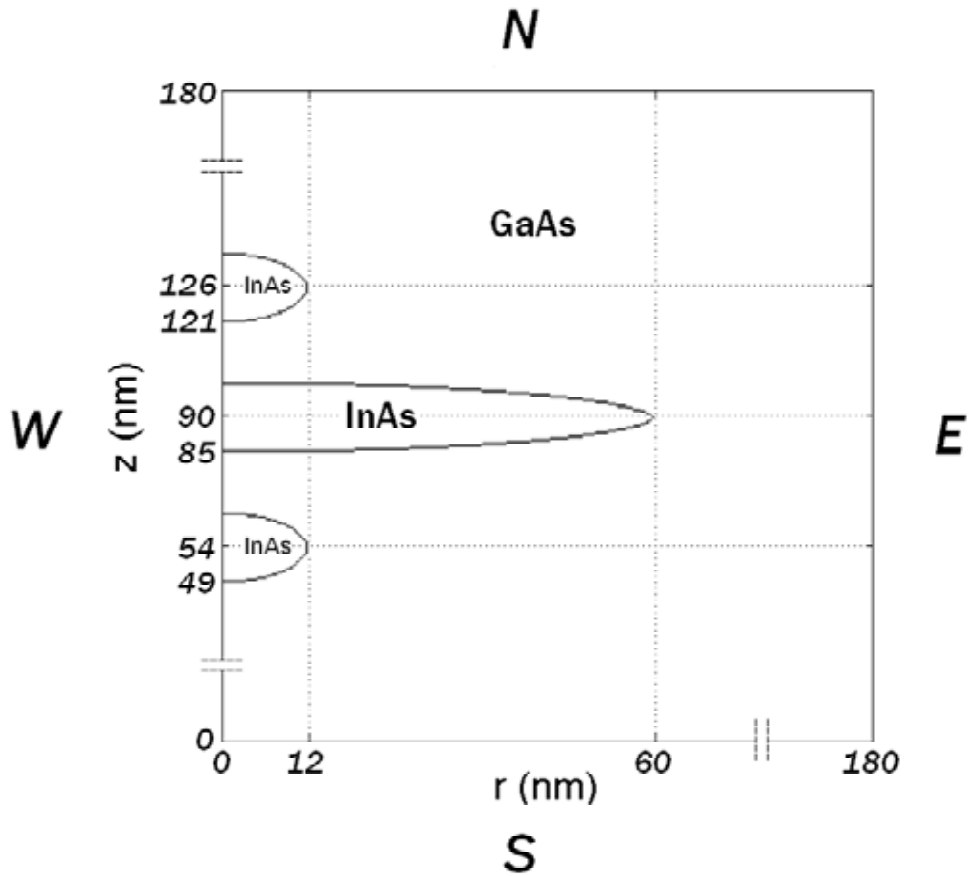
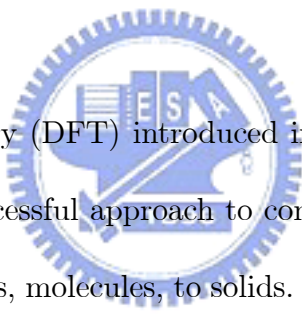


Figure 1.1: Three vertically aligned InAs/GaAs quantum dots with cylindrically symmetric domain in real space dimensions in nano meters that are used in numerical implementation. The domain in 2D setting is denoted by Ω with the boundary $\partial\Omega$ consisting of the south (S), east (E), north (N), and west (W) sides.

Chapter 2

The Current Spin Density Functional Theory for the Model System



The density functional theory (DFT) introduced in the two seminal papers [26] [27] is perhaps the most successful approach to compute the electronic structure of matter ranging from atoms, molecules, to solids. Vignale and Rasolt developed an extension of DFT that makes it possible to include gauge fields in the energy functional [15] [16] and has been widely used to describe the electronic structure of quantum dots in magnetic fields [17] [18] [19] [28].

In CSDF, the ground state energy of an interacting system with electron number N and the total spin S in the local external potential $V_{ext}(\mathbf{r})$ is a functional of spin density $n^\sigma(\mathbf{r})$, with $\sigma = \uparrow, \downarrow$ (or ± 1) denoting spin-up and spin-down, respectively,

$$E(n) = T(n) + \int n(\mathbf{r}) \left[V_{ext}(\mathbf{r}) + \frac{1}{2} V_H(\mathbf{r}) \right] d\mathbf{r} + E_B(n) + E_{xc}(n), \quad (2.1)$$

where the total density $n(\mathbf{r}) = n^\uparrow(\mathbf{r}) + n^\downarrow(\mathbf{r})$ and the spin densities satisfy the constraint $\int n^\sigma(\mathbf{r}) d\mathbf{r} = N^\sigma$ with $N^\uparrow = (N + 2S)/2$, and $N^\downarrow = (N - 2S)/2$ [28]. Assuming that the ground state of the noninteracting reference system is nondegenerate, the noninteracting kinetic energy is expressed as

$$T(n) = \sum_{j,\sigma} \left\langle \Psi_{j\sigma} \left| \Pi \left(\frac{1}{2m(\mathbf{r}, \varepsilon_{j\sigma})} \right) \Pi \right| \Psi_{j\sigma} \right\rangle, \quad (2.2)$$

where $\Pi = -i\hbar\nabla + e\mathbf{A}(\mathbf{r})$ denotes the electron momentum operator, \hbar is the reduced Planck constant, e is the proton charge, $\mathbf{A}(\mathbf{r}) = \frac{B}{2}(-y, x, 0)$ is the vector potential induced by an external magnetic field $\mathbf{B} = \text{curl } \mathbf{A} = B\hat{z}$ applied perpendicular to the xy plane, and $\Psi_{j\sigma}$ and $\varepsilon_{j\sigma}$ are Kohn-Sham (KS) orbitals and eigenvalues to be specified below. The effect of band nonparabolicity leads to the mass depending on both energy and position, which is defined by [20]

$$\frac{1}{m(\mathbf{r}, \varepsilon_{j\sigma})} = \frac{p^2}{\hbar^2} \left[\frac{2}{\varepsilon_{j\sigma} + E_g(\mathbf{r}) - V_{ext}(\mathbf{r})} + \frac{1}{\varepsilon_{j\sigma} + E_g(\mathbf{r}) - V_{ext}(\mathbf{r}) + \Delta(\mathbf{r})} \right], \quad (2.3)$$

where $E_g(\mathbf{r})$ and $\Delta(\mathbf{r})$ are energy-band gap and spin-orbit splitting in the valence band, respectively, and p is the momentum matrix element. These parameters are material (position) dependent. We denote the spatial domain of the model, i.e., Fig. 1.1, as $\bar{\Omega} = \bar{\Omega}_{InAs} \cup \bar{\Omega}_{GaAs} \subset R^3$, where the three *InAs* quantum dots are

embedded in the *GaAs* matrix. All numerical values of the parameters used in this thesis are listed in Table 1, which also includes the corresponding units and cited references.

Table 1. Numerical values of all parameters used in this thesis.

	value	unit	formula	reference
e	1.60219×10^{-19}	J		
B		T		
\hbar	1.05459×10^{-34}	$J\cdot s$		
p (InAs)	1.20311×10^{-28}		$3m_0p^2/\hbar^2$	[29]
p (GaAs)	1.25614×10^{-28}			
m_0	9.10956×10^{-31}	kg		
E_g (InAs)	0.421	eV		[29]
E_g (GaAs)	1.52	eV		[29]
Δ (InAs)	0.48	eV		[29]
Δ (GaAs)	0.34	eV		[29]
V_0	0.77	eV		[29]
ϵ_0	8.854187×10^{-12}	F/m		
ϵ_{InAs}	12.2			[20]
ϵ_{GaAs}	12.7			
μ_B	9.2741×10^{-24}	J/T		
c	2.997925×10^8	m/s		

The hard-wall confinement potential V_{ext} is induced by a discontinuity of conduction-band edge of the system components and is given as

$$V_{ext}(\mathbf{r}) = \begin{cases} 0, & \text{in } \bar{\Omega}_{InAs} \\ V_0, & \text{in } \bar{\Omega}_{GaAs}. \end{cases} \quad (2.4)$$

The Hartree potential is defined as

$$V_H(\mathbf{r}) = \frac{e^2}{4\pi\epsilon_0\epsilon(\mathbf{r})} \int \frac{n(\mathbf{r}')}{|\mathbf{r} - \mathbf{r}'|} d\mathbf{r}', \quad (2.5)$$

where ϵ_0 the permittivity of vacuum and $\epsilon(\mathbf{r})$ is the dielectric constant of the background material.

The vector field $\mathbf{A}(\mathbf{r})$ adds extra terms to the energy functional as follows

$$E_B(n) = \frac{1}{2}g\mu_B B \int [n^\uparrow(\mathbf{r}) - n^\downarrow(\mathbf{r})] d\mathbf{r} + e \int \mathbf{j}_p(\mathbf{r}) \cdot \mathbf{A}(\mathbf{r}) d\mathbf{r}, \quad (2.6)$$

where g is the Landé factor, μ_B is the Bohr magneton, and

$$\mathbf{j}_p(\mathbf{r}) = \frac{-i\hbar}{2m} \sum_{j,\sigma} [\Psi_{j\sigma}^*(\mathbf{r}) \nabla \Psi_{j\sigma}(\mathbf{r}) - \Psi_{j\sigma}(\mathbf{r}) \nabla \Psi_{j\sigma}^*(\mathbf{r})]$$

is the paramagnetic current density.

The xc energy $E_{xc}(n)$ is defined as

$$E_{xc}(n) = E_x(n) + E_c(n) = \int n(\mathbf{r}) \varepsilon_{xc}(n, \gamma) d\mathbf{r}, \quad (2.7)$$

where the xc energy per particle ε_{xc} depends on the field B . This is a consequence of the fact that the external field changes the internal structure of the wave function. It formally depends on the vorticity

$$\gamma(\mathbf{r}) = \nabla \times \frac{\mathbf{j}_p(\mathbf{r})}{n(\mathbf{r})} \Big|_z. \quad (2.8)$$

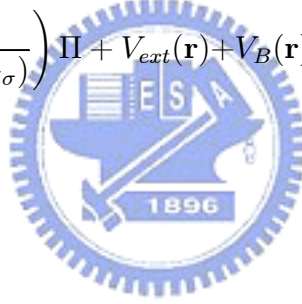
To minimize the total energy of the system, a functional derivative of $E(n)$ is taken with respect to $\Psi_{j\sigma}^*$ under the constraint of the orbitals $\Psi_{j\sigma}$ being normalized. The resulting KS equations are

$$\mathbf{H}_{KS}^\sigma \Psi_{j\sigma} = \varepsilon_{j\sigma} \Psi_{j\sigma} \quad (2.9)$$

with the KS Hamiltonian \mathbf{H}_{KS}^σ defined as

$$\mathbf{H}_{KS}^\sigma = -\Pi \left(\frac{1}{2m(\mathbf{r}, \varepsilon_{j\sigma})} \right) \Pi + V_{ext}(\mathbf{r}) + V_B(\mathbf{r}) + V_H(\mathbf{r}) + V_{xc}^\sigma(\mathbf{r}), \quad (2.10)$$

where



$$V_B(\mathbf{r}) = \sigma \frac{1}{2} g(\mathbf{r}, \varepsilon_{j\sigma}) \mu_B B, \quad (2.11)$$

$$g(\mathbf{r}, \varepsilon_{j\sigma}) = 2 \left\{ 1 - \frac{m_0}{m(\mathbf{r}, \varepsilon_{j\sigma})} \frac{\Delta(\mathbf{r})}{3(\varepsilon_{j\sigma} + E_g(\mathbf{r}) - V_{ext}(\mathbf{r})) + 2\Delta(\mathbf{r})} \right\}, \quad (2.12)$$

and $\sigma = \pm 1$ referring to the orientation of the electron spin along the z axis. The xc potential

$$V_{xc}^\sigma(\mathbf{r}) = \frac{\delta [n(\mathbf{r}) \varepsilon_{xc}(n, \gamma)]}{\delta n^\sigma} - \frac{e}{n} \mathbf{j}_p \cdot \mathbf{A}_{xc}, \quad (2.13)$$

where \mathbf{A}_{xc} is the xc vector potential defined by

$$e\mathbf{A}_{xc} = \frac{1}{n} \left(\frac{\partial}{\partial y} \frac{\delta [n(\mathbf{r})\varepsilon_{xc}(n, \gamma)]}{\delta \gamma}, -\frac{\partial}{\partial x} \frac{\delta [n(\mathbf{r})\varepsilon_{xc}(n, \gamma)]}{\delta \gamma}, 0 \right). \quad (2.14)$$

We use the LSDA for calculating the xc energy. In CSDFT, the LSDA has to be extended to include the orbital currents. Following Vignale and Rasolt [16], the xc vector potential is approximated as

$$\frac{e}{c}\mathbf{A}_{xc,\sigma} \approx \frac{-\bar{b}}{n_\sigma(\mathbf{r})} \nabla \times \left[\nabla \times \frac{\mathbf{j}_{p\sigma}(\mathbf{r})}{n_\sigma(\mathbf{r})} \right], \quad (2.15)$$

where

$$-\bar{b} = \frac{mk_F}{48\pi^2} \left[\frac{\chi_L}{\chi_L^0} - 1 \right] \quad (2.16)$$

with k_F being the Fermi momentum and $\frac{\chi_L}{\chi_L^0}$ the diamagnetic-susceptibility ratio. The values of this ratio are tabulated in [30].

For the xc energy functional ε_{xc} in (2.13), we adopt the form developed by Perdew and Wang [31] as

$$\varepsilon_{xc}^{PW}(n, \zeta) = \varepsilon_x(r_s, \zeta) + \varepsilon_c(r_s, \zeta) \quad (2.17)$$

where

$$\begin{aligned} \varepsilon_x(r_s, \zeta) &= -\frac{3}{4\pi r_s} \left[\frac{9\pi}{4} \right]^{1/3} \frac{[(1+\zeta)^{4/3} + (1-\zeta)^{4/3}]}{2}, \\ \varepsilon_c(r_s, \zeta) &= \varepsilon_c(r_s, 0) + \alpha_c(r_s) \frac{f(\zeta)}{f''(0)} (1 - \zeta^4) \end{aligned} \quad (2.18)$$

$$+ [\varepsilon_c(r_s, 1) - \varepsilon_c(r_s, 0)] f(\zeta) \zeta^4, \quad (2.19)$$

$\zeta = (n^\uparrow(\mathbf{r}) - n^\downarrow(\mathbf{r})) / n(\mathbf{r})$ is the spin polarization, $r_s = \left(\frac{3}{4\pi n}\right)^{1/3}$ is the Wigner-Seitz radius, and the functions $\varepsilon_c(r_s, 0)$, $\varepsilon_c(r_s, 1)$, and $-\alpha_c(r_s)$ are given in [31]. Note that the magnetic field dependence on the correlation energy, which might affect the total energies and spin configurations, is not taken into account in the present formula.



Chapter 3

Numerical Methods and Algorithms for the Model System

Since the three QDs and the magnetic field are cylindrically symmetric, the wave function, the spin density, and the paramagnetic current density can be represented as

$$\Psi_q(\mathbf{r}) = e^{-il\theta} \phi_q(r, z), \quad q \equiv \{nl\sigma\} \quad (3.1)$$

$$n^\sigma(\mathbf{r}) = n^\sigma(r, z) = \sum_q^{N^\sigma} |\phi_q(r, z)|^2, \quad (3.2)$$

$$\mathbf{j}_p(\mathbf{r}) = -\frac{\hbar}{m(r, z, \varepsilon_q)} \sum_q^N l |\phi_q(r, z)|^2 \hat{\mathbf{e}}_\theta, \quad (3.3)$$

where n is the principal quantum number, $l = 0, \pm 1, \pm 2, \dots$, is the quantum number of the projection of angular momentum onto the magnetic field axis, i.e., the z -axis and $\hat{\mathbf{e}}_\theta$ is the azimuthal unit vector. The KS equations are then reduced to a 2D problem in the (r, z) coordinates as

$$\mathbf{H}_{KS}^{l\sigma} \phi_q(r, z) = \varepsilon_q \phi_q(r, z), \quad (3.4)$$

where the KS Hamiltonian is now defined by

$$\mathbf{H}_{KS}^{l\sigma} = T_S + T_B + V_{ext} + V_B + V_H + V_{xc} \quad (3.5)$$

$$T_S(r, z) = -\frac{\hbar^2}{2m(r, z, \varepsilon_q)} \left(\frac{\partial^2}{\partial r^2} + \frac{1}{r} \frac{\partial}{\partial r} - \frac{l^2}{r^2} + \frac{\partial^2}{\partial z^2} \right) \quad (3.6)$$

$$T_B(r, z) = \frac{e^2 B^2 r^2}{8m(r, z, \varepsilon_q)} + \frac{\hbar e B l}{2m(r, z, \varepsilon_q)}. \quad (3.7)$$

In 2D setting, the solution domain for (3.4) is again expressed by the same notation as that of 3D, that is, $\bar{\Omega} = \bar{\Omega}_{InAs} \cap \bar{\Omega}_{GaAs} \subset R^2$. We choose the domain $\bar{\Omega}_{GaAs}$ sufficiently large so that the wave function is negligibly small at the boundary of $\bar{\Omega}_{GaAs}$. By symmetry, the domain $\bar{\Omega}$ can be reduced to $\bar{\Omega} = \{(r, z) : 0 \leq r \leq r_{\max}, -z_{\max} \leq z \leq z_{\max}\}$ for sufficiently large $r_{\max} > 0$ and $z_{\max} > 0$ as shown in Fig. 1.1.

The explicit formula for the potential $V_{xc}(\mathbf{r})$ in (2.13) is extremely complex in 3D coordinates. Transforming it to the (r, z) space is prohibitively lengthy and impractical. We use all the original formulas (2.13)-(2.19) for calculating $V_{xc}(\mathbf{r})$ in the 3D space and then obtain the potential in the (r, z) coordinates, i.e., $V_{xc}(r, z)$ for (3.4).

Since we are dealing with the hard-wall confinement potential, the interface conditions of the wave function in (3.4) has to be specifically imposed, namely,

$$\begin{cases} \frac{1}{2m(r, z, \varepsilon_q)} \Pi \phi_q(r, z) \cdot \mathbf{n} \Big|_{\Gamma^-} = \frac{1}{2m(r, z, \varepsilon_q)} \Pi \phi_q(r, z) \cdot \mathbf{n} \Big|_{\Gamma^+}, \\ \phi_q(r, z) \Big|_{\Gamma^-} = \phi_q(r, z) \Big|_{\Gamma^+}, \end{cases} \quad (3.8)$$

where Γ denotes the interface between two materials, i.e., $\Gamma = \overline{\Omega}_{InAs} \cap \overline{\Omega}_{GaAs}$, \mathbf{n} is an outward normal unit vector on the boundary of Ω_{InAs} , and Γ^- and Γ^+ are the sets of limiting points to the curve Γ from the interior and the exterior of Ω_{InAs} , respectively. The momentum operator Π is similarly defined for the 2D case. The boundary conditions for (3.4) are

$$\begin{cases} \frac{\partial \phi_q(r,z)}{\partial r} \Big|_W = 0, \\ \phi_q(r,z) = 0, \text{ on } S, E, N, \end{cases} \quad (3.9)$$

where W , S , E , and N denotes the west, south, east, and north side boundaries of the domain $\overline{\Omega}$. Note that on the west side of the boundary the values of the wave function are taken to be the same for satisfying the continuity condition across W . In actual implementation this condition is replaced by taking the values of the two horizontal grid points adjacent to W as the same. Moreover, to avoid numerical over-flow due to the term $1/r$ in (3.6), we do not define unknowns at the grid points on W .

Note that the potential functions $V_{ext}(\mathbf{r})$ and $V_B(\mathbf{r})$ can be directly reduced to the (r, z) space since these functions are independent of the azimuthal coordinate. In real space approximation, the Hartree potential $V_H(\mathbf{r})$ is usually calculated by solving the Poisson equation [32]

$$\nabla \cdot \epsilon(\mathbf{r}) \nabla V_H(\mathbf{r}) = -\frac{e^2}{4\pi\epsilon_0} n(\mathbf{r}). \quad (3.10)$$

By cylindrical symmetry, this equation can be written as

$$\left(\frac{\partial^2}{\partial r^2} + \frac{1}{r} \frac{\partial}{\partial r} + \frac{1}{r^2} \frac{\partial^2}{\partial \theta^2} + \frac{\partial^2}{\partial z^2} \right) V_H(r, \theta, z) = f(r, z), \quad (3.11)$$

$$f(r, z) = -\frac{e^2}{4\pi\epsilon_0\epsilon_i} \sum_q^N |\phi_q(r, z)|^2, \text{ for } i = 1 \text{ or } 2, \quad (3.12)$$

where $\epsilon_1 = \epsilon_{InAs}$ if $(r, z) \in \overline{\Omega}_{InAs}$ and $\epsilon_2 = \epsilon_{GaAs}$ if $(r, z) \in \overline{\Omega}_{GaAs}$. By using the method of separating variables and substituting a solution of the form

$$V_H(r, \theta, z) = V_H(r, z) V(\theta) \quad (3.13)$$

into (3.11), we have

$$V(\theta) \left(\frac{\partial^2}{\partial r^2} + \frac{1}{r} \frac{\partial}{\partial r} + \frac{\partial^2}{\partial z^2} \right) V_H(r, z) + V_H(r, z) \frac{1}{r^2} \frac{\partial^2 V(\theta)}{\partial \theta^2} = f(r, z)$$

or

$$\frac{V(\theta)r^2}{V_H(r, z)} \left(\frac{\partial^2}{\partial r^2} + \frac{1}{r} \frac{\partial}{\partial r} + \frac{\partial^2}{\partial z^2} \right) V_H(r, z) + \frac{\partial^2 V(\theta)}{\partial \theta^2} = \frac{r^2}{V_H(r, z)} f(r, z). \quad (3.14)$$

Obviously, by setting $V(\theta) = k$ where k is an arbitrary constant, a function $V_H^p(r, z) = kV_H(r, z)$ satisfying the 2D Poisson equation

$$\left(\frac{\partial^2}{\partial r^2} + \frac{1}{r} \frac{\partial}{\partial r} + \frac{\partial^2}{\partial z^2} \right) V_H^p(r, z) = f(r, z) \quad (3.15)$$

is a particular solution of (3.14) in view of a second order nonhomogeneous ordinary differential equation with respect to θ . The corresponding homogeneous general solution is $e^{ik\theta} V_H^h(r, z)$ satisfying the Laplace equation

$$\left(\frac{\partial^2}{\partial r^2} + \frac{1}{r} \frac{\partial}{\partial r} + \frac{\partial^2}{\partial z^2} - \frac{k^2}{r^2} \right) V_H^h(r, z) = 0. \quad (3.16)$$

The general solution of the nonhomogeneous equation (3.14) is therefore of the form

$$\sum_k e^{ik\theta} V_H^h(r, z) + V_H^p(r, z). \quad (3.17)$$

In 2D setting, we also have similar interface conditions for Poisson's problem (3.10), namely,

$$\begin{cases} \epsilon(r, z) \nabla V_H^p(r, z) \cdot \mathbf{n}|_{\Gamma^-} = \epsilon(r, z) \nabla V_H^p(r, z) \cdot \mathbf{n}|_{\Gamma^+}, \\ V_H(r, z)|_{\Gamma^-} = V_H(r, z)|_{\Gamma^+}. \end{cases} \quad (3.18)$$

Similarly, the boundary conditions for (3.10) are

$$\begin{cases} \frac{\partial V_H^p(r, z)}{\partial r} \Big|_W = 0, \\ V_H^p(r, z) = 0, \text{ on } S, E, N. \end{cases} \quad (3.19)$$

By imposing these boundary conditions to the general solution (3.17), we deduce that the particular solution $V_H^p(r, z)$ is in fact a general solution of (3.14) and thus of (3.11), i.e., $V_H^h(r, z) = 0$.

Note that for atomic systems the far side boundary condition of the Hartree potential is usually taken the values obtained by using efficient multipole expansion techniques [33]. For our model problem, the size of the domain is $180 \times 180 \text{ nm}^2$ which in comparison with that of atomic systems is quite large and hence

the zero boundary condition for the potential on the far side of the boundary is numerically feasible, see Chapter. 4 below for numerical evidence on the choice of the size.

We then use the standard finite difference method to approximate our model problem. Since the mass in (2.3) and the Landé factor of (2.12) are energy dependent, the KS equation (3.4) and its interface and boundary conditions (3.8) and (3.9) will result in a system of cubic eigenvalue equations

$$\left(A_0 + \lambda A_1 + \lambda^2 A_2 + \lambda^3 A_3\right) \mathbf{x} = 0, \quad (3.20)$$

where the unknown eigenpair (λ, \mathbf{x}) is an approximate solution of (ε_q, ϕ_q) for some q . Starting from the Schrödinger equation, finite difference discretization, to the coefficient matrices $A_0, A_1, A_2,$ and $A_3,$ a detailed derivation of a similar cubic eigenvalue system is given in Appendix (or[24]). Several Jacobi-Davidson methods are proposed and compared in [25] for solving this type of eigenvalue problems.

Analogously, the Poisson equation (3.15) with its interface and boundary conditions (3.18) and (3.19) leads to a system of algebraic equations

$$A\mathbf{x} = \mathbf{b}, \quad (3.21)$$

where now the unknown vector \mathbf{x} corresponds to the approximate values of $V_H(r, z)$ at the grid points.

We briefly describe our algorithm for the implementation of the model system

in CSDFT as follows:

Algorithm 1. A self-consistent method for the current spin density functional theory.

- (1) Set $V_H = 0$, $V_{xc} = 0$, and solve (3.20) for $\phi_q^{(0)}(r, z)$ with $\sigma = \uparrow$ and then with $\sigma = \downarrow$ by using the cubic Jacobi-Davidson method. Set $k = 0$. When $B = 0$, the first three lowest energies correspond to $n = 1$ and $l = 0, 1, 2$. We therefore must solve (3.20) six times. At each time, we only seek for the smallest eigenpair. As for $B = 15$, the first three lowest energies correspond to $n = 1, 2, 3$ and $l = 0$. We thus solve (3.20) two times. At each time, we then seek for the three smallest eigenpairs.
- (2) Evaluate the electron densities $n^\uparrow(\mathbf{r})$, $n^\downarrow(\mathbf{r})$, $n(\mathbf{r})$, and the electron energies $E_q^{(k)}$. If the energies converge within an error tolerance then stop. Otherwise, set $k = k + 1$.
- (3) Solve (3.21) for the Hartree potential V_H by using GMRES [34].
- (4) Evaluate V_{xc} via (2.13) and then solve (3.20) for the next iterate $\phi_q^{(k)}(r, z)$.
Go to (2).

There are several numerical issues deserved to be elaborated due to the special formulation of the present model when compared with the existing models of multielectronic systems of QDs. The most prominent feature of the present model is the nonparabolic dispersion relation used to define the effective mass (2.3), the

Landé factor (2.12), and the interface condition (3.8). As a result, the set of eigenvalues that interests us is embedded in the interior of the spectrum of the eigenvalue problem (3.20) which is a nonsymmetric system. Moreover, with some feasible magnetic fields, we expect to have degenerate eigenstates due to the two identical smaller dots, i.e., the eigenvalue system is defective. Instead of using deflation scheme in the JD solver [25], we extend the generalized Davidson method of Crouzeix, Philippe, and Sadkane [35] to our cubic JD method that allows us to compute several eigenpairs simultaneously and to have a block implementation of Krylov subspaces and search direction transformation. Our JD algorithm is summarized as follows:

Algorithm 2. A cubic Jacobi-Davidson method.

- (1) Choose an arbitrary orthonormal matrix $V := [v_1, \dots, v_n]$ and let K be a given integer that limits the dimension of the basis of the subspace. Here n can be taken as 3 for six electrons with spin-up and spin-down.
- (2) Compute $W_k = A_k V$ and $M_k = V^* W_k$, for $k = 0, 1, 2, 3$, where the matrices A_k are given in (3.20).
- (3) For $j = n, \dots, K$, do
 - (3a) Compute the eigenpairs of $(\theta^3 M_3 + \theta^2 M_2 + \theta M_1 + M_0)\phi = 0$ by solving the generalized linear eigenvalue problem

$$\begin{bmatrix} 0 & I & 0 \\ 0 & 0 & I \\ M_0 & M_1 & M_2 \end{bmatrix} \begin{bmatrix} s \\ \theta s \\ \theta^2 s \end{bmatrix} = \theta \begin{bmatrix} I & & \\ & I & \\ & & -M_3 \end{bmatrix} \begin{bmatrix} s \\ \theta s \\ \theta^2 s \end{bmatrix}$$

using the QZ algorithm [36].

- (3b) Select the desired eigenpairs (θ_i, ϕ_i) with $\|\phi_i\|_2 = 1$, for $i = 1, \dots, n$.
- (3c) For $i = 1, \dots, n$, compute the Ritz vectors $u_i = V\phi_i$, the residuals $r_i = A(\theta_i)u_i$, and $p_i = A'(\theta_i)u_i$, where $A(\theta_i) := A_0 + \theta_i A_1 + \theta_i^2 A_2 + \theta_i^3 A_3$ and $A'(\theta_i) := A_1 + 2\theta_i A_2 + 3\theta_i^2 A_3$.
- (3d) If $\|r_i\|_2 < Tol$, for $i = 1, \dots, n$, then stop.
- (3e) If $K - j < n$, then go to Step (4).
- (3f) For $i = 1, \dots, n$, do
- If $\|r_i\|_2 < Tol$, then go to Step (3f).
 - Compute the correction $t = -M_A^{-1}r_i + \varepsilon M_A^{-1}$, where $\varepsilon = \frac{u_i^* M_A^{-1} r_i}{u_i^* M_A^{-1} p_i}$ and M_A is a preconditioner (by SSOR) of $A(\theta_i)$.
 - Orthonormalize t against V by the modified Gram-Schmidt (MGS) method.
 - For $k = 0, 1, 2, 3$, compute $w_k = A_k t$, $M_k = \begin{bmatrix} M_k & V^* w_k \\ t^* W_k & v^* w_k \end{bmatrix}$.
 - Expand $V = [V, t]$ and $W_k = [W_k, w_k]$, for $k = 0, 1, 2, 3$.
 - Set $j = j + 1$.

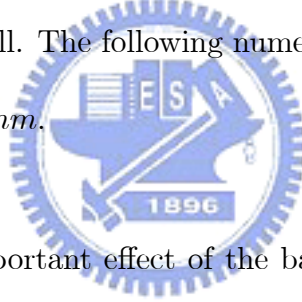
- (4) Use n Ritz vectors u_1, \dots, u_n to create a new $V := MGS(u_1, \dots, u_n)$ and go to Step (2) for restarting.

Note that the classical approach for dealing with the nonlinear matrix equation (3.20) is to transform the equation into a generalized linear eigenvalue system with the matrix dimension of 3 times that of (3.20) and then solve the system by the Lanczos or Arnoldi method. The matrix dimension of (3.20) for the present QDM model is about 290000. The JD method described here instead solves the generalized linear eigenvalue system in Step (3a) in a much smaller subspace V . The matrix dimension of the matrices M_i , $i = 0, 1, 2, 3$, is about 50 in our numerical implementation. The matrix dimension of the linearized system in Step (3a) is thus about 150. The KS Hamiltonian (2.10) is based on the nonparabolic band structure approximation. If the Hamiltonian is based on the Kane's original form, the resulting eigenvalue problem will then be of linear form but with the matrix dimension of 4 times that of (3.20). The nonparabolic approximation thus reduces computational efforts significantly at the cost of more delicate nonlinear eigenvalue systems.

Chapter 4

Numerical Results

For the proposed model, we first determine the size of the domain in Fig. 1.1 by inspecting the rate of change of the first three energy levels with respect to $r_{\max} = z_{\max}$. As shown in Fig. 4.1, the change of these energies around $r_{\max} = 180nm$ and beyond is relatively small. The following numerical results are thus based on the domain with $r_{\max} = 180nm$.



We next present the important effect of the band nonparabolicity. In Table 2, we observe that the energy differences between the parabolic and nonparabolic dispersion relations used in the Hamiltonian for zero magnetic field can be very significant since the magnitudes are comparable with that of the correlation energies as shown in Table 3. For the parabolic dispersion case, the effective mass in (2.2) is taken as $m = 0.024m_0$. In Tables 3 and 4, all energy components in (3.5) are separately presented to indicate the magnitudes of the energies from various effects. Here, the total ground-state energy E obtained via the KS eigenvalues ε_q is defined by [16]

$$\begin{aligned}
E &= \sum_q^N E_q = \sum_q^N \varepsilon_q - \frac{1}{2} \frac{e^2}{4\pi\epsilon_0\epsilon(\mathbf{r})} \int \int \frac{n(\mathbf{r})n(\mathbf{r}')}{|\mathbf{r} - \mathbf{r}'|} d\mathbf{r}' d\mathbf{r} \\
&\quad - \sum_\sigma \int V_{xc}^\sigma(\mathbf{r})n^\sigma(\mathbf{r})d\mathbf{r} - \frac{e}{c} \int \mathbf{j}_p \cdot \mathbf{A}_{xc} d\mathbf{r} + E_{xc}(n).
\end{aligned}$$

Table 2. Energies for the nonparabolic and parabolic approximation at $B = 0$ in units of eV .

$q = \{nl\sigma\}$	nonparabolic	parabolic
$\{1, 0, +1\}$	0.094673	0.086873
$\{1, 1, +1\}$	0.102689	0.095749
$\{1, 2, +1\}$	0.112039	0.106298

Table 3. Energies at $B = 0$ in units of eV .

q	$\{1, 0, +1\}$	$\{1, 1, +1\}$	$\{1, 2, +1\}$
E_q	0.094673	0.102689	0.112039
$\langle T_S \rangle$	0.067484	0.075638	0.084511
$\langle T_B \rangle$	0	0	0
$\langle V_{ext} \rangle$	0.019227	0.020536	0.022024
E_B	0	0	0
$\frac{1}{2} \langle V_H \rangle$	0.015120	0.013653	0.012280
E_x	-0.006772	-0.006753	-0.006398
E_c	-0.000386	-0.000385	-0.000378

Table 4. Energies at $B = 15$ in units of eV .

E_q^* are energies based on the single-particle Hamiltonian.

q	$\{1, 0, +1\}$	$\{2, 0, +1\}$	$\{3, 0, +1\}$	$\{1, 0, -1\}$	$\{2, 0, -1\}$	$\{3, 0, -1\}$
E_q^*	0.103250	0.134668	0.134668	0.114840	0.146072	0.146072
E_q	0.113092	0.146387	0.147649	0.120784	0.153012	0.154220
$\langle T_S \rangle$	0.078144	0.114168	0.113827	0.077302	0.113209	0.112880
$\langle T_B \rangle$	0.008975	0.002510	0.002499	0.008889	0.002484	0.002473
$\langle V_{ext} \rangle$	0.017801	0.021184	0.021067	0.017713	0.021108	0.020994
E_B	-0.004436	-0.003913	-0.003877	0.004325	0.003832	0.003798
$\frac{1}{2} \langle V_H \rangle$	0.021932	0.026358	0.028058	0.021925	0.026359	0.028059
E_x	-0.008884	-0.013414	-0.013418	-0.008877	-0.013419	-0.013422
E_c	-0.000441	-0.000506	-0.000506	-0.000493	-0.000562	-0.000562

As stated above, our main concern for the present QDM model is to show the state change of the electrons under the influence of magnetic fields. The wave functions of the six electrons originally occupying the lowest 3 energy states with $B = 0$ as given in Table 3 are shown in the left panel of Fig. 4.2, which clearly illustrates that the electrons are residing in the central dot. For $B = 15$, we see that, corresponding to the lowest 6 energy states as given in Table 4, each one of these three dots contains two electrons for which their wave functions are shown in the right panel of Fig. 4.2. Note that three dimensional wave functions can be easily illustrated from these two dimensional wave functions via the formula (3.1).

Accuracy of the exchange energies can be verified by the ratio between the absolute values of $\frac{1}{2} \langle V_H \rangle$ and E_x , which is about 2 for two-electron atoms [37]. It has been theoretically shown in [38] that this ratio is exactly equal to 2 for a two-electron model for which the xc energy and xc potential can be determined exactly in an external harmonic potential. From Tables 3 and 4, the ratio is approximately 2.

Finally, we remark that the essential physics of this study, namely the state change of electrons in QDM under the influence of magnetic field as such indicated by Fig. 4.2, can also be simulated by means of a much simpler model, e.g., the single-particle Hamiltonian with parabolic band structure (i.e., constant effective mass approximation). However, the numerics of the computed energies can be quite different from that of the present model as shown by the numbers in the second and third rows in Table 4. Moreover, we may obtain degenerate states such as $\{2, 0, +1\}$ and $\{3, 0, +1\}$ under the single-particle picture, which obviously is incorrect. In addition to the effect of the model in use, the state change is significantly governed by the QDM dimensions as given in Fig. 1.1 so that we can attain the electronic behavior as shown in Fig. 4.2. These dimensions are also experimentally feasible [9].

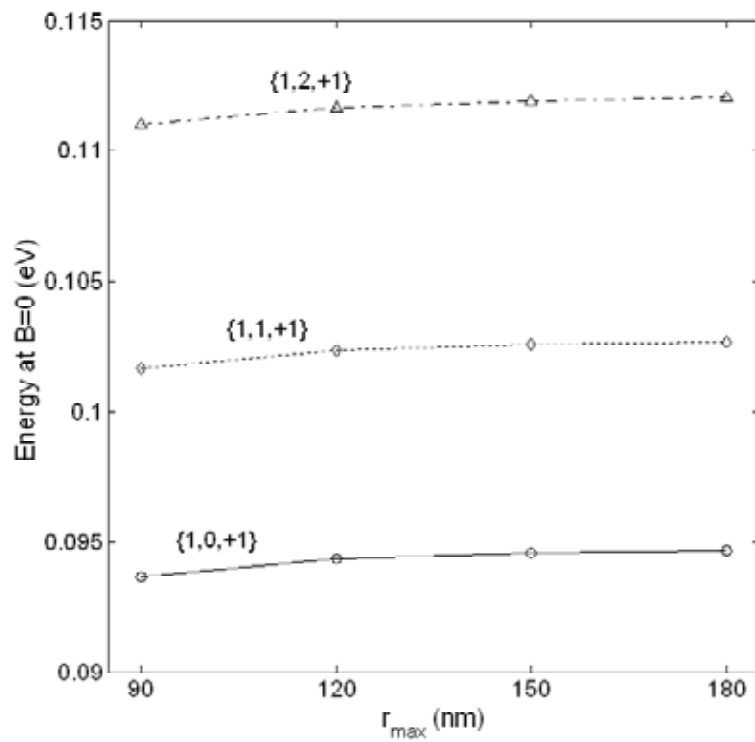


Figure 4.1: The effect of the domain size on the first three energies at $B = 0$.

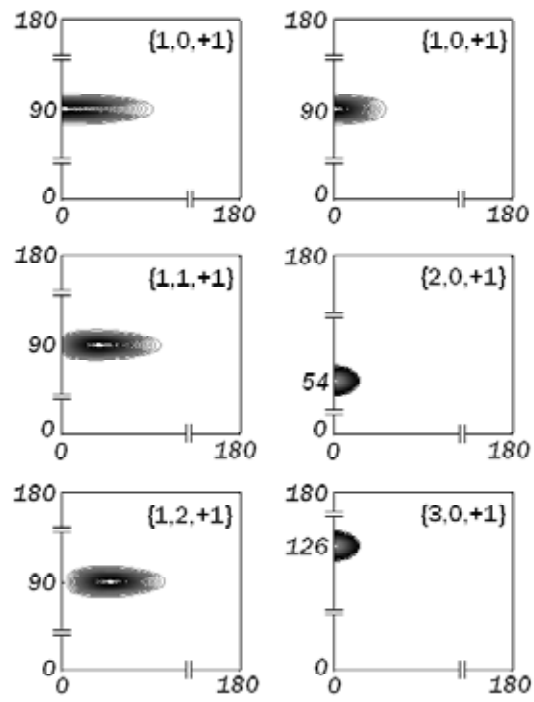


Figure 4.2: Contour of KS orbitals at $B=0$ (left panel) and $B=15$ (right panel).

Chapter 5

Concluding Remarks

A new mathematical model that incorporates the nonparabolic energy dispersion relation and realistic hard-wall finite confinement potential into the many-body Hamiltonian in the current spin density functional theory in 3D setting is proposed. It is used to study the electronic properties of a quantum dot molecule that consists of three vertically aligned semiconductor quantum dots (one large central dot and two smaller identical dots) under the influence of magnetic fields. A new Jacobi-Davidson method is given to solve the cubic eigenvalue problem resulting from finite difference approximation due to the nonparabolic nature of the effective mass. It is shown that the effect of band nonparabolicity can be very significant in the sense that the energy difference between the parabolic and nonparabolic cases is comparable with that of correlation energies in multielectronic system. Furthermore, we show that six electrons residing in the large central dot at zero magnetic field can be changed to such that each dot contains two electrons with some feasible magnetic field.

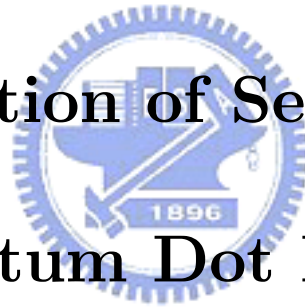
This thesis is intended to describe mathematical aspects of the model and to present preliminary physical results only on the Kohn-Sham orbitals and detailed

energy components with two different magnetic fields. Following this more realistic and accurate model, there are many interesting physical phenomena such as capacitance, optical and transport properties, Wigner crystallization, Aharonov-Bohm oscillation, and quantum Hall effect can be further investigated for semiconductor nanostructures in three dimensional space. In particular, with an additional electric control, we expect to have an energy selective mechanism to manipulating excitonic states of two closely spaced QDMs so that a strong coherent dipole-dipole coupling can be achieved and hence the Förster-Dexter resonant energy transfer between QDMs can be realized to motivate a new paradigm of Fermionic qubits for quantum computing in solid-state systems.



Part II

A Numerical Method for Exact Diagonalization of Semiconductor Quantum Dot Model



Chapter 6

Introduction

Exact diagonalization of many-body Hamiltonian is the most accurate and expensive method to study the electron dynamics and correlation in a semiconductor QD [44] [46] [47] [50] [51] [53] [28] [62]. Efficient methods such as the Hartree-Fock method and density functional approach are known to give substantial errors in energy, many-body wave function, spin-polarized states, and exchange-correlation potentials etc. [38] [46] [47] [50] [52].

Most of the theoretical models for QDs are based on 2D electron gas systems with parabolic infinite confinement potential, which are justifiable for calculating single-particle states, addition energy spectra, and many qualitatively new features of QDs. In fact, 2D models have turned out to be surprisingly rich and difficult [28]. However, the Coulomb interaction between electrons in QDs is three dimensional by nature and is the most important effect of many-body dynamics in QDs. It has been shown in [43] [54] that 2D models often lead to an inadequate description of the Coulomb interaction as a consequence of the overestimated carrier localization. The 3D models are found to reproduce the experimental data for a large class of QD structures where simplified 2D models may fail [41] [45]

[48] [54].

There is another issue concerning the accuracy of QD models, namely, the effective-mass approximation (EMA) which allows us to model the conduction electrons in a QD as a decoupled interacting system with one-band effective mass from their environment that consists of millions of atoms in crystalline structure. This assumption makes numerous theoretical investigations possible within tolerable computing resources. Most of the existing models are based on the parabolic EMA. In [45], the QD model with nonparabolic EMA is shown to describe quantitatively the capacitance-voltage and far-infrared measurement data. The model does estimate correctly the change in the effective mass due to the nonparabolic effect. Moreover, it is shown in [49] that the effect of band nonparabolicity can be very significant in the sense that the energy difference between the parabolic and nonparabolic cases is comparable with that of exchange energies in multielectronic system.

In addition to the computational complexity compounded greatly by the three dimensionality and the exact diagonalization, the nonparabolicity leads to nonlinear (cubic) eigenvalue problems with interior eigenvalues which are much harder to solve than that of linear eigenvalue problems [40] [25] [22] [56] [59] [24]. In this paper, we propose a numerical algorithm for exact diagonalization of the many-electron Hamiltonian of a disk-shaped 3D *InAs/GaAs* QD model with nonparabolic EMA. The algorithm consists of the advanced cubic Jacobi-Davidson

method developed in [25] [49], GMRES, a model reduction technique for both Schrödinger and Poisson equations, and a new numerical approach to the exact diagonalization.

The computation of all pair-wise Coulomb interactions is one of the limiting factors in *ab initio* electronic structure calculations [57]. Our model reduction technique is a consequence of cylindrical symmetry of the model. This technique allows us to calculate the Coulomb matrix elements within tolerable accuracy and computing times. The reduction technique is not meant for general purposes but for a test of our idea on the numerical exact diagonalization.

Since the states of a QD are localized in space, the plan-wave approach for 2D electron gas systems would require a very large number of Fourier components to define a localized state [43]. Another approach that has been developed to reduce the number of basis states is to construct the single-particle basis functions that are separable into an in-plane (parallel to the radial axis) and a perpendicular part. The Fock-Darwin states (associated with Laguerre polynomials) are a good choice for in-plane states because they are the eigenstates of parabolically confined electrons [42] [43] [53] [58]. The perpendicular, or subband, functions are determined numerically by solving a 1D Hartree-Fock equation. The many-electron system is then solved by minimizing the total energy of all conduction electrons in the system in a function space spanned by a basis of multi-electron functions which are constructed as a direct antisymmetrized product of single-particle basis

functions. To achieve a convergence for a few-electron system, the size of the single-particle basis functions must be of the order of a million [53].

These approaches are not suitable for the model considered in this paper due to the hard-wall confinement potential and the nonparabolic EMA. We present here a fully numerical approach for the exact diagonalization of many-electron Hamiltonian. In our approach, the basis set of single-particle functions is obtained by solving the cubic eigenvalue problem resulting from a finite difference approximation of the single-electron QD model. The eigenvalue problem is solved by the block cubic Jacobi-Davidson method proposed in [49]. Since the single-particle spectrum depends on the hard-wall confinement potential which is finite, the size of the basis set will have an upper limit. The use of single-particle basis will thus reduce the computational cost without losing accuracy on the ground state energy of the whole system. Compared with other approaches, the trade-off of our approach is the solution of the cubic eigenvalue problem with the size of tens of thousands.

We briefly summarize the main results of our approach as follows. For a 4-electron QD with the hard-wall confinement potential taken as $V_0 = 0.77 \text{ eV}$ (electron volts), we only need $12 \sim 16$ single-particle states to obtain a convergent ground state energy within meV (milli-electron volts) accuracy. The computational complexity of calculating all pair-wise Coulomb interactions is $C_2^{N_s} + N_s$ where $C_2^{N_s}$ is the binomial coefficient of N_s (the number of single-particle states)

and 2, i.e., we need to solve the Poisson equation $C_2^{N_s} + N_s$ times for this particular system.

The single-electron nonparabolic EMA model is given in the following chapter. Numerical methods for this model are briefly described in Chapter 8. We refer to [25] [24] for more mathematical details on the discretization of the model and the solution of the cubic eigenvalue problem. In Chapter 9, we introduce our exact diagonalization approach to the many-electron system. The special point to note is the construction of the basis set of multi-electron wave functions based on the single-electron functions. A simple example is given to illustrate the function space definition. In Chapter 10, we present the model reduction technique and numerical methods for calculating Coulomb matrix elements. An overall algorithm for the solution procedure of the many-electron system is summarized in this chapter as well. Numerical results are presented in Chapter 11. Finally, we make some concluding remarks in the last chapter.

Chapter 7

Single-Electron Model

Let the spatial domain of the QD model considered herein be a disk-shaped $\bar{\Omega} = \bar{\Omega}_{InAs} \cup \bar{\Omega}_{GaAs} \subset R^3$ as shown by a cross section of $\bar{\Omega}$ in Fig. 7.1 where the *InAs* QD is embedded in the *GaAs* matrix whose dimensions are commensurable with that of [9] in which a transmission electron micrograph of a QD sample is illustrated. Within the nonparabolic EMA, the Hamiltonian for an electron in the QD is given by

$$H_0(\mathbf{r}) = \frac{-\hbar^2}{2} \nabla_{\mathbf{r}} \left(\frac{1}{m(\mathbf{r}, \varepsilon)} \right) \nabla_{\mathbf{r}} + V_c(\mathbf{r}) \quad (7.1)$$

$$V_c(\mathbf{r}) = \begin{cases} 0, & \text{in } \bar{\Omega}_{InAs} \\ V_0, & \text{in } \bar{\Omega}_{GaAs} \end{cases} \quad (7.2)$$

$$\frac{1}{m(\mathbf{r}, \varepsilon)} = \frac{p^2}{\hbar^2} \left[\frac{2}{\varepsilon + E_g(\mathbf{r}) - V_c(\mathbf{r})} + \frac{1}{\varepsilon + E_g(\mathbf{r}) - V_c(\mathbf{r}) + \Delta(\mathbf{r})} \right] \quad (7.3)$$

where $\nabla_{\mathbf{r}}$ stands for the spatial gradient, ε is the electron (unknown) energy, \hbar is the reduced Planck constant, $E_g(\mathbf{r})$ is the energy-band gap, $\Delta(\mathbf{r})$ is the spin-orbit splitting in the valence band, p is the momentum matrix element, and m_0 is the free electron mass. Note particularly that the nonparabolic effective mass $m(\mathbf{r}, \varepsilon)$

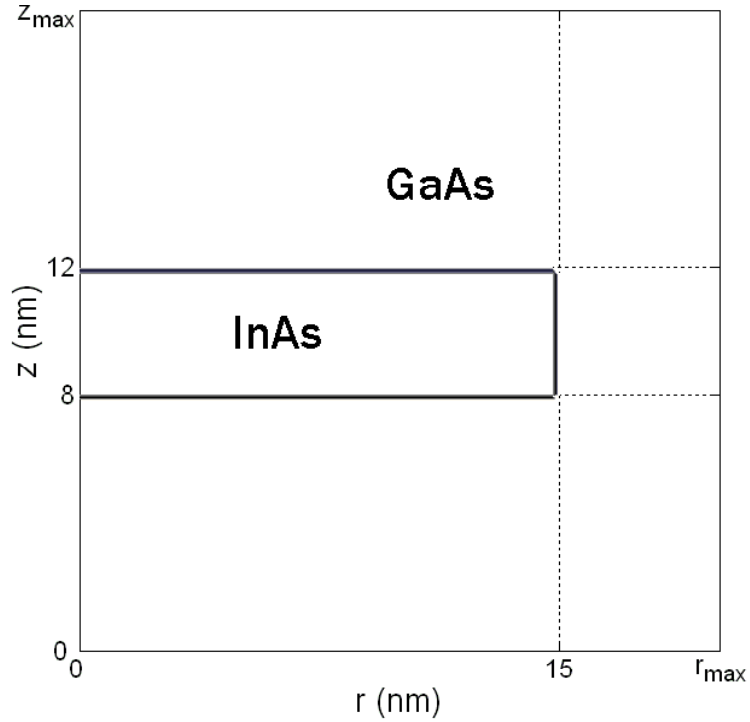


Figure 7.1: A cross section of a disk-shaped *InAs* quantum dot embedded in the *GaAs* matrix in real space dimensions in nano meters that are used in numerical implementation.

depends on both position and electron energy and that the hard-wall confinement potential V_c is induced by a discontinuity of conduction-band edges of *InAs* and *GaAs*. All numerical values of the parameters used in this paper are listed in Table 1 which also includes the corresponding units and cited references.

Chapter 8

Numerical Methods for Single Electron Wave Functions

To obtain the states of the many-body system, we begin by solving the single particle problem

$$H_0\Phi = \varepsilon\Phi. \quad (8.1)$$

Due to cylindrical symmetry, the envelope wave functions $\Phi(\mathbf{r})$ of this problem can be expressed as

$$\Phi_q(\mathbf{r}) = e^{-il\theta}\phi_q(r, z), \quad q \equiv \{nl\}, \quad (8.2)$$

where n is the principal quantum number, and $l = 0, \pm 1, \pm 2, \dots$ is the quantum number of the projection of angular momentum onto the z -axis. Eq. (8.1) can then be reduced to a 2D problem in the (r, z) coordinates as

$$H_0\phi_q(r, z) = \varepsilon_q\phi_q(r, z), \quad (8.3)$$

where the Hamiltonian H_0 is now defined by

$$H_0 = -\frac{\hbar^2}{2m(r, z, \varepsilon_q)} \left(\frac{\partial^2}{\partial r^2} + \frac{1}{r} \frac{\partial}{\partial r} - \frac{l^2}{r^2} + \frac{\partial^2}{\partial z^2} \right) + V_c(r, z) \quad (8.4)$$

In 2D setting, the solution domain for (8.3) is again expressed by the same notation as that of 3D, that is, $\bar{\Omega} = \bar{\Omega}_{InAs} \cap \bar{\Omega}_{GaAs} \subset R^2$. We choose the domain $\bar{\Omega}_{GaAs}$ sufficiently large so that the wave function is negligibly small at the boundary of $\bar{\Omega}_{GaAs}$. By symmetry, the domain $\bar{\Omega}$ can be reduced to $\bar{\Omega} = \{(r, z) : 0 \leq r \leq r_{\max}, 0 \leq z \leq z_{\max}\}$ for sufficiently large $r_{\max} > 0$ and $z_{\max} > 0$ as shown in Fig. 7.1.

Since we are dealing with the hard-wall confinement potential, the interface conditions of the wave function in (8.3) has to be specifically imposed, namely,

$$\begin{cases} \frac{1}{m(r, z, \varepsilon_q)} \nabla \phi_q(r, z) \cdot \mathbf{n} \Big|_{\Gamma^-} = \frac{1}{m(r, z, \varepsilon_q)} \nabla \phi_q(r, z) \cdot \mathbf{n} \Big|_{\Gamma^+}, \\ \phi_q(r, z) \Big|_{\Gamma^-} = \phi_q(r, z) \Big|_{\Gamma^+}, \end{cases} \quad (8.5)$$

where Γ denotes the interface between two materials, i.e., $\Gamma = \bar{\Omega}_{InAs} \cap \bar{\Omega}_{GaAs}$, \mathbf{n} is an outward normal unit vector on the boundary of Ω_{InAs} , and Γ^- and Γ^+ are the sets of limiting points to the curve Γ from the interior and the exterior of Ω_{InAs} , respectively. The momentum operator ∇ is similarly defined for the 2D case. The boundary conditions for (8.4) are

$$\begin{cases} \frac{\partial \phi_q(r, z)}{\partial r} \Big|_W = 0, \\ \phi_q(r, z) = 0, \text{ on } S, E, N, \end{cases} \quad (8.6)$$

where W , S , E , and N denotes the west, south, east, and north side boundaries of

the domain $\bar{\Omega}$. Note that on the west side of the boundary the values of the wave function are taken to be the same for satisfying the continuity condition across W . In actual implementation this condition is replaced by taking the values of the two horizontal grid points adjacent to W as the same. Moreover, to avoid numerical over-flow due to the term $1/r$ in (8.4), we do not define unknowns at the grid points on W .

We then use the standard finite difference method to approximate the model problem. Since the mass in (7.3) is energy dependent, Eqs. (8.3), (8.5), and (8.6) result in a system of cubic eigenvalue equations

$$\left(A_0 + \lambda A_1 + \lambda^2 A_2 + \lambda^3 A_3\right) \mathbf{x} = 0, \quad (8.7)$$

where the unknown eigenpair (λ, \mathbf{x}) is an approximate solution of (ε_q, ϕ_q) for some q at grid points. Starting from the Schrödinger equation, finite difference discretization, to the coefficient matrices A_0 , A_1 , A_2 , and A_3 , a detailed derivation of the same cubic eigenvalue system is given in Appendix (or[24]). Several Jacobi-Davidson methods are proposed and compared in [25] for solving this type of eigenvalue problems.

Chapter 9

Many-Electron Model

To describe a system of N electrons in a QD under the influence of the Coulomb interaction, we write the total Hamiltonian H as a sum of single-particle operators H_i and two-body operators V_{ij} in the envelope-function approximation as

$$H = \sum_{i=1}^N H_i + \frac{1}{2} \sum_{i \neq j} V_{ij} \quad (9.1)$$

$$H_i = H_0(\mathbf{r}_i) \quad (9.2)$$

$$V_{ij} = V_C(\mathbf{r}_i, \mathbf{r}_j) = \frac{e^2}{4\pi\epsilon_0\epsilon(\mathbf{r}_i) |\mathbf{r}_i - \mathbf{r}_j|} \quad (9.3)$$

where the single-electron Hamiltonian $H_0(\mathbf{r}_i)$ is defined as (7.1) for the i th electron and e is the proton charge. For the sake of simplicity in exposition, the mutual interaction between the electrons in the system is taken to be purely Coulombic.

From single-particle picture to many-particle picture for QDs, we follow the theoretical framework developed by Pietiläinen and Chakraborty in [53]. The approximate eigen-pairs (ε_q, ϕ_q) form a single-particle basis set

$$B = \{|\Phi_q\rangle = |q\rangle : q = 1, 2, \dots, N_s\}. \quad (9.4)$$

From this set, a basis B_N for N interacting electrons in a QD can be constructed as a direct antisymmetrized product of B of the form

$$B_N = \mathcal{A} \bigotimes_{j=1}^N B = \{|Q_i\rangle : i = 1, 2, \dots, N_m\}, \quad (9.5)$$

where N_s is the total number of computed single-particle states, \mathcal{A} denotes the antisymmetrization operator, and $N_m = C_N^{N_s}$. More specifically, the many-body basis functions $|Q_i\rangle$ are Slater determinants defined as

$$\begin{aligned} |Q_i\rangle &= \mathcal{A}[|q_{i_1}\rangle \otimes |q_{i_2}\rangle \cdots \otimes |q_{i_N}\rangle] \\ &= \frac{1}{\sqrt{N!}} \begin{vmatrix} \Phi_{q_{i_1}}(\mathbf{r}_1) & \Phi_{q_{i_2}}(\mathbf{r}_1) & \cdots & \Phi_{q_{i_N}}(\mathbf{r}_1) \\ \Phi_{q_{i_1}}(\mathbf{r}_2) & \Phi_{q_{i_2}}(\mathbf{r}_2) & \cdots & \Phi_{q_{i_N}}(\mathbf{r}_2) \\ \vdots & \vdots & \ddots & \vdots \\ \Phi_{q_{i_1}}(\mathbf{r}_N) & \Phi_{q_{i_2}}(\mathbf{r}_N) & \cdots & \Phi_{q_{i_N}}(\mathbf{r}_N) \end{vmatrix}. \end{aligned} \quad (9.6)$$

The states of the interacting system are then expressed by the superposition of the non-interacting states (9.5) as

$$|\Psi\rangle = \sum_{i=1}^{N_m} c_i |Q_i\rangle, \quad (9.7)$$

where the unknown coefficients c_i are sought by minimizing the energy functional

$$\langle \Psi | H | \Psi \rangle \quad (9.8)$$

with respect to c_i subject to the normalization condition

$$\langle \Psi | \Psi \rangle = 1. \quad (9.9)$$

An Example

We now illustrate the above formalism by considering a simple case as follows:

$$N = 2, N_s = 3 \quad (9.10)$$

$$B = \{|\Phi_q\rangle : q = 1, 2, 3\} \quad (9.11)$$

$$N_m = C_2^3 = \frac{3!}{2!1!} = 3 \quad (9.12)$$

$$B_2 = \mathcal{A} \bigotimes_{q=1}^2 B = \{ |Q_i\rangle : i = 1, 2, \dots, N_m \} \quad (9.13)$$

$$|Q_1\rangle = |q_1; q_2\rangle = \frac{1}{\sqrt{2}} \begin{vmatrix} \Phi_1(\mathbf{r}_1) & \Phi_2(\mathbf{r}_1) \\ \Phi_1(\mathbf{r}_2) & \Phi_2(\mathbf{r}_2) \end{vmatrix} \quad (9.14)$$

$$|Q_2\rangle = |q_1; q_3\rangle = \frac{1}{\sqrt{2}} \begin{vmatrix} \Phi_1(\mathbf{r}_1) & \Phi_3(\mathbf{r}_1) \\ \Phi_1(\mathbf{r}_2) & \Phi_3(\mathbf{r}_2) \end{vmatrix} \quad (9.15)$$

$$|Q_3\rangle = |q_2; q_3\rangle = \frac{1}{\sqrt{2}} \begin{vmatrix} \Phi_2(\mathbf{r}_1) & \Phi_3(\mathbf{r}_1) \\ \Phi_2(\mathbf{r}_2) & \Phi_3(\mathbf{r}_2) \end{vmatrix} \quad (9.16)$$

$$|\Psi\rangle = \sum_{j=1}^3 c_j |Q_j\rangle \quad (9.17)$$

$$\langle \Psi | H | \Psi \rangle = \iint d\mathbf{r}_1 d\mathbf{r}_2 \left(\sum_{i=1}^3 c_i |Q_i\rangle^* \right) H \left(\sum_{j=1}^3 c_j |Q_j\rangle \right) \quad (9.18)$$

$$\langle \Psi | \Psi \rangle = \iint d\mathbf{r}_1 d\mathbf{r}_2 |\Psi(\mathbf{r}_1, \mathbf{r}_2)|^2 = 1 \quad (9.19)$$

Using the method of Lagrange multipliers, the minimization of (9.8) subject to (9.9) leads to

$$\frac{\partial}{\partial c_i} \{ \langle \Psi | H | \Psi \rangle - \lambda \langle \Psi | \Psi \rangle \} = 0, \quad i = 1, 2, 3, \quad (9.20)$$

$$\begin{aligned} \frac{\partial}{\partial c_i} \langle \Psi | H | \Psi \rangle &= \iint d\mathbf{r}_1 d\mathbf{r}_2 |Q_i\rangle^* H \left(\sum_{j=1}^3 c_j |Q_j\rangle \right) \\ &+ \iint d\mathbf{r}_1 d\mathbf{r}_2 \left(\sum_{j=1}^3 c_j |Q_j\rangle^* \right) H |Q_i\rangle \end{aligned} \quad (9.21)$$

$$\frac{\partial}{\partial c_i} \lambda \langle \Psi | \Psi \rangle = 2\lambda \sum_{j=1}^3 c_j \iint d\mathbf{r}_1 d\mathbf{r}_2 |Q_i\rangle^* |Q_j\rangle \quad (9.22)$$

$$H_{ij} = \langle Q_i | H | Q_j \rangle = \left\langle Q_i \left| H_1 + H_2 + \frac{1}{2} V_{12} \right| Q_j \right\rangle \quad (9.23)$$

$$\langle Q_2 | H_1 | Q_3 \rangle = \iint d\mathbf{r}_1 d\mathbf{r}_2 Q_2^* H_1 Q_3 \quad (9.24)$$

$$\begin{aligned} &= \frac{1}{2} \iint d\mathbf{r}_1 d\mathbf{r}_2 [\Phi_1^*(\mathbf{r}_1) \Phi_3^*(\mathbf{r}_2) - \Phi_1^*(\mathbf{r}_2) \Phi_3^*(\mathbf{r}_1)] H_1 \\ &[\Phi_2(\mathbf{r}_1) \Phi_3(\mathbf{r}_2) - \Phi_2(\mathbf{r}_2) \Phi_3(\mathbf{r}_1)] \end{aligned} \quad (9.25)$$

$$\begin{aligned} &= \frac{1}{2} \iint d\mathbf{r}_1 d\mathbf{r}_2 [\Phi_1^*(\mathbf{r}_1) \Phi_3^*(\mathbf{r}_2) - \Phi_1^*(\mathbf{r}_2) \Phi_3^*(\mathbf{r}_1)] \\ &[\Phi_3(\mathbf{r}_2) H_1 \Phi_2(\mathbf{r}_1) - \Phi_2(\mathbf{r}_2) H_1 \Phi_3(\mathbf{r}_1)] \end{aligned} \quad (9.26)$$

$$\begin{aligned} \langle Q_2 | H_2 | Q_3 \rangle &= \frac{1}{2} \iint d\mathbf{r}_1 d\mathbf{r}_2 [\Phi_1^*(\mathbf{r}_1) \Phi_3^*(\mathbf{r}_2) - \Phi_1^*(\mathbf{r}_2) \Phi_3^*(\mathbf{r}_1)] \\ &[\Phi_2(\mathbf{r}_1) H_2 \Phi_3(\mathbf{r}_2) - \Phi_3(\mathbf{r}_1) H_2 \Phi_2(\mathbf{r}_2)] \end{aligned} \quad (9.27)$$

$$\begin{aligned} \left\langle Q_2 \left| \frac{1}{2} V_{12} \right| Q_3 \right\rangle &= \frac{1}{4} \iint d\mathbf{r}_1 d\mathbf{r}_2 [\Phi_1^*(\mathbf{r}_1) \Phi_3^*(\mathbf{r}_2) - \Phi_1^*(\mathbf{r}_2) \Phi_3^*(\mathbf{r}_1)] \frac{e^2}{4\pi\epsilon_0\epsilon(\mathbf{r}_1)} \\ &\quad \frac{1}{|\mathbf{r}_1 - \mathbf{r}_2|} [\Phi_2(\mathbf{r}_1) \Phi_3(\mathbf{r}_2) - \Phi_2(\mathbf{r}_2) \Phi_3(\mathbf{r}_1)] \end{aligned} \quad (9.28)$$

$$\begin{bmatrix} H_{11} & H_{12} & H_{13} \\ H_{21} & H_{22} & H_{23} \\ H_{31} & H_{32} & H_{33} \end{bmatrix} \begin{bmatrix} c_1 \\ c_2 \\ c_3 \end{bmatrix} = \lambda \begin{bmatrix} c_1 \\ c_2 \\ c_3 \end{bmatrix} \quad (9.29)$$

Therefore, the total energy of N electrons in the QD can be obtained by diagonalizing the linear eigenvalue problem

$$\sum_{j=1}^{N_m} (H_{ij} - \lambda\delta_{ij}) c_j = 0, \quad (9.30)$$

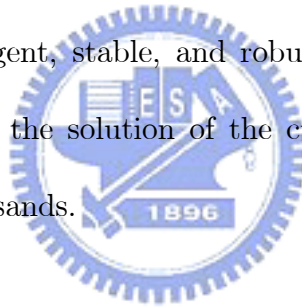
where the eigenvectors $\mathbf{c} = [c_1 \ c_2 \ \cdots \ c_{N_m}]^T$ are the desired expansion coefficients and the eigenvalues λ the corresponding energies of the interacting system.

The finite confinement potential leads to a finite number of localized states as well as to energetically higher delocalized states. When the influence of the delocalized states on the discrete QD spectrum is neglected, the eigenvalue problem (9.30) has a finite dimension and can be solved without further approximations. The most computationally expensive part is the calculation of the Coulomb matrix elements (9.28) whereas the other parts (9.26) and (9.27) can be directly calculated from (8.7) or equivalently from (8.3).

Obviously, the computational complexity is essentially determined by N_s which in turn is limited by the confinement potential strength V_0 in (7.2). This is the

main difference between our approach and the others such as those in [43] [42] [53] [58] where the size of the single-particle basis (analytical) functions must be of the order of a million owing to the approximation by means of either the 2D electron gas modeling or the subband structure. We also note that the choice of analytical functions, e.g. Laguerre polynomials, for the single-particle basis is not feasible for our model because of the finite and local nature of the confinement potential V_0 and the nonlinear dependence of the effective mass $m(\mathbf{r},\varepsilon)$ on both position and electron energy. In fact, the evaluation of Coulomb matrix elements by using Laguerre polynomials is numerically highly unstable owing to large terms of alternating sign in the polynomial [53].

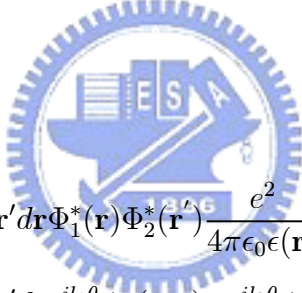
Our approach is convergent, stable, and robust (see below). However, the trade-off of our approach is the solution of the cubic eigenvalue problem (8.7) with the size of tens of thousands.



Chapter 10

Numerical Methods for Coulomb Matrix Elements

Since the basis states $|Q_i\rangle$ have been constructed by diagonalizing H_0 , we are left to compute the Coulomb matrix elements defined by the two-body operator V_C of (9.3) as


$$\langle 12|V_C|34\rangle = \iint d\mathbf{r}' d\mathbf{r} \Phi_1^*(\mathbf{r}) \Phi_2^*(\mathbf{r}') \frac{e^2}{4\pi\epsilon_0\epsilon(\mathbf{r})} \frac{1}{|\mathbf{r} - \mathbf{r}'|} \Phi_3(\mathbf{r}) \Phi_4(\mathbf{r}') \quad (10.1)$$

$$= \iint d\mathbf{r}' d\mathbf{r} e^{il_1\theta} \phi_1(r, z) e^{-il_3\theta} \phi_3(r, z) \frac{e^2}{4\pi\epsilon_0\epsilon(\mathbf{r})} \frac{1}{|\mathbf{r} - \mathbf{r}'|} e^{il_2\theta'} \phi_2(r', z') e^{-il_4\theta'} \phi_4(r', z'), \quad (10.2)$$

for any arbitrary states $\Phi_i(\mathbf{r})$, $i = 1, 2, 3, 4$, representing four-center two-electron repulsion integrals. For real space approximation, we define a potential-like function $V_{24}(\mathbf{r})$ as

$$V_{24}(\mathbf{r}) = \frac{e^2}{4\pi\epsilon_0\epsilon(\mathbf{r})} \int \frac{e^{il_2\theta'} \phi_{24}(r', z')}{|\mathbf{r} - \mathbf{r}'|} d\mathbf{r}' \quad (10.3)$$

where $l_{24} = l_2 - l_4$ and $\phi_{24}(r', z') = \phi_2(r', z') \phi_4(r', z')$. This function can then be cast into a Poisson equation

$$\nabla \cdot \epsilon(\mathbf{r}) \nabla V_{24}(\mathbf{r}) = -\frac{e^2}{4\pi\epsilon_0} e^{il_{24}\theta} \phi_{24}(r, z). \quad (10.4)$$

By cylindrical symmetry, this equation can be written as

$$\left(\frac{\partial^2}{\partial r^2} + \frac{1}{r} \frac{\partial}{\partial r} + \frac{1}{r^2} \frac{\partial^2}{\partial \theta^2} + \frac{\partial^2}{\partial z^2} \right) V_{24}(r, \theta, z) = e^{il_{24}\theta} f(r, z), \quad (10.5)$$

$$f(r, z) = -\frac{e^2}{4\pi\epsilon_0\epsilon_i} \phi_{24}(r, z), \text{ for } i = 1 \text{ or } 2, \quad (10.6)$$

where $\epsilon_1 = \epsilon_{InAs}$ if $(r, z) \in \overline{\Omega}_{InAs}$ and $\epsilon_2 = \epsilon_{GaAs}$ if $(r, z) \in \overline{\Omega}_{GaAs}$. By using the method of separating variables and substituting a solution of the form

$$V_{24}(r, \theta, z) = V_{24}(r, z) V_{24}(\theta) \quad (10.7)$$

into (10.5), we have

$$e^{-il_{24}\theta} V_{24}(\theta) \left(\frac{\partial^2}{\partial r^2} + \frac{1}{r} \frac{\partial}{\partial r} + \frac{\partial^2}{\partial z^2} \right) V_{24}(r, z) \\ + e^{-il_{24}\theta} V_{24}(r, z) \frac{1}{r^2} \frac{\partial^2 V_{24}(\theta)}{\partial \theta^2} = f(r, z)$$

or

$$\frac{e^{-il_{24}\theta} V_{24}(\theta) r^2}{V_{24}(r, z)} \left(\frac{\partial^2}{\partial r^2} + \frac{1}{r} \frac{\partial}{\partial r} + \frac{\partial^2}{\partial z^2} \right) V_{24}(r, z)$$

$$+e^{-il_{24}\theta} \frac{\partial^2 V_{24}(\theta)}{\partial \theta^2} = \frac{r^2}{V_{24}(r, z)} f(r, z). \quad (10.8)$$

Obviously, the function $V_{24}^p(\theta) = e^{il_{24}\theta}$ is a particular solution of (10.8) if we view (10.8) as a second order nonhomogeneous ordinary differential equation with respect to θ provided that there exists a function $V_{24}^p(r, z)$ satisfying the 2D Poisson equation

$$\left(\frac{\partial^2}{\partial r^2} + \frac{1}{r} \frac{\partial}{\partial r} + \frac{\partial^2}{\partial z^2} - \frac{l_{24}^2}{r^2} \right) V_{24}^p(r, z) = f(r, z). \quad (10.9)$$

This implies that $V_{24}^p(r, \theta, z) = V_{24}^p(r, z) V_{24}^p(\theta)$ is a particular solution of (10.5).

The general solution of the corresponding homogeneous equation is thus $e^{ik\theta} V_{24}^h(r, z)$

such that $V_{24}^h(r, z)$ satisfies the Laplace equation

$$\left(\frac{\partial^2}{\partial r^2} + \frac{1}{r} \frac{\partial}{\partial r} + \frac{\partial^2}{\partial z^2} - \frac{k^2}{r^2} \right) V_{24}^h(r, z) = 0 \quad (10.10)$$

for any integer k . The general solution of the nonhomogeneous equation (10.8)

(or (10.5)) is therefore of the form

$$\sum_k e^{ik\theta} V_{24}^h(r, z) + V_{24}^p(r, z). \quad (10.11)$$

In 2D setting, we also have interface conditions for Poisson's problem, namely,

$$\begin{cases} \epsilon(r, z) \nabla V_{24}^p(r, z) \cdot \mathbf{n}|_{\Gamma^-} = \epsilon(r, z) \nabla V_{24}^p(r, z) \cdot \mathbf{n}|_{\Gamma^+}, \\ V_{24}(r, z)|_{\Gamma^-} = V_{24}(r, z)|_{\Gamma^+}. \end{cases} \quad (10.12)$$

Similarly, the boundary conditions for (10.4) are

$$\begin{cases} \left. \frac{\partial V_{24}^p(r,z)}{\partial r} \right|_W = 0, \\ V_{24}^p(r,z) = 0, \text{ on } S, E, N. \end{cases} \quad (10.13)$$

By imposing these boundary conditions to the general solution (10.11), we deduce that the particular solution $V_{24}^p(r,z)$ is in fact a general solution of (10.8) and thus of (10.5), i.e., $V_{24}^h(r,z) = 0$. This implies that $V_{24}(r,\theta,z) = e^{il_{24}\theta} V_{24}^p(r,z)$ is a general solution of (10.4).

Consequently, we have

$$\langle 12|V_c|34 \rangle = \int \Phi_1^*(\mathbf{r}) \Phi_3(\mathbf{r}) e^{il_{24}\theta} V_{24}^p(r,z) d\mathbf{r} \quad (10.14)$$

$$= \int_0^{2\pi} e^{i(l_{13}-l_{42})\theta} d\theta \int \int \phi_{13}(r,z) V_{24}^p(r,z) r dr dz \quad (10.15)$$

$$= 2\pi \delta_{l_{13}l_{42}} \int \int \phi_{13}(r,z) V_{24}^p(r,z) r dr dz \quad (10.16)$$

where the computation of the 3D Coulomb matrix element (10.1) is reduced to solving the 2D problem (10.9).

Again the finite difference method is used for solving the Poisson problem (10.9), (10.12), and (10.13). This leads to a system of algebraic equations

$$\mathbf{Ax} = \mathbf{b}, \quad (10.17)$$

where now the unknown vector \mathbf{x} corresponds to the approximate values of $V_{24}^p(r,z)$ at the grid points.

We summarize the above methods for studying the electronic properties of few interacting electrons confined in a QD via exact diagonalization as follows.

An Exact Diagonalization Algorithm:

- (0) Set the number of electrons N and the number of single-particle states N_s .

The number of many-body basis functions $N_m = C_N^{N_s}$.

- (1) Solve the single-particle problem (8.1) in discrete form (8.7) for N_s basis functions by means of the cubic Jacobi-Davidson method for some principal quantum numbers n and angular momentum quantum numbers l (8.2) which are determined by N_s .

- (2) Use the N_s basis functions to construct N_m Slater determinants (9.6).

- (3) Evaluate Coulomb matrix elements (10.16) by solving the Poisson problem (10.9), (10.12), (10.13) in discrete form (10.17) via GMRES [34].

- (4) Solve the eigenvalue problem (9.30) for the lowest eigenvalue (ground state energy) and the corresponding eigenvector of the N -electron system by using the QR algorithm [36].

Chapter 11

Numerical Results

Since Coulomb interaction has a long-range tail, the computational domain must be sufficiently large. We first determine the size of the domain in Fig. 7.1 by inspecting the rate of change of the ground state energy with respect to $r_{\max} = z_{\max}$ for a 2-electron system with $N_s = 8$. As shown in Fig. 11.1, the change of the ground state energy around $r_{\max} = 100 \text{ nm}$ and beyond is relatively small. The following numerical results are thus based on the domain with $r_{\max} = 100 \text{ nm}$. On the $(100,100) \text{ nm}^2$ domain, we set 151 nonuniform grid points [24] along each direction for the finite difference approximation.

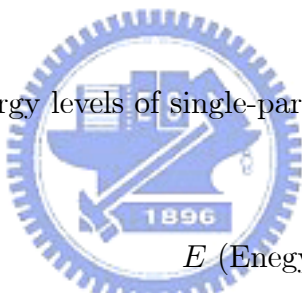
In order to have a sufficiently large basis set B (9.4), it is necessary to solve (8.4) with various l from 0 to -4 . Some smallest positive real eigenvalues and their associated eigenvectors of (8.7) are computed for each l . Some of the first low-lying energy levels of the single-electron system are shown in Table 5. If all these states are taken to be the basis of B , then $N_s = 8$.

The ground state energies of 2 and 4 electrons with various basis numbers N_s are shown in Table 6 and plotted in Fig. 11.2. It is clear that the many-electron QD can be modeled to a very good precision with the energy down to the order of

milli-electron volts (meV) by using just few tens of single-particle basis functions. The convergence behavior of the ground state energy with respect to the basis size N_s of our approach is also clearly demonstrated by the figure.

The computational complexity increases quadratically with N_s . For example, for the case of $N_s = 18$, we need to solve the Poisson problem, i.e., the linear system (10.17) $C_2^{18} + 18 = 171$ times for Coulomb matrix elements. Nevertheless, all of our numerical methods for solving the systems (8.7), (9.30), and (10.17) are stable and convergent.

Table 5. The first 8 energy levels of single-particle system for B (9.4).



q (State)	n	l	E (Energy in eV)
1	1	0	0.248189
2	1	-1	0.275593
3	1	-2	0.309664
4	2	0	0.321248
5	1	-3	0.348811
6	2	-1	0.371052
7	1	-4	0.391899
8	2	-2	0.424284

Table 6. Ground state energies of N -electron system
with respect to N_s .

N	N_s	λ (eV)
2	12	0.530213
2	14	0.530046
2	16	0.529667
2	18	0.529667
4	12	1.192199
4	14	1.185846
4	16	1.184708
4	18	1.182987



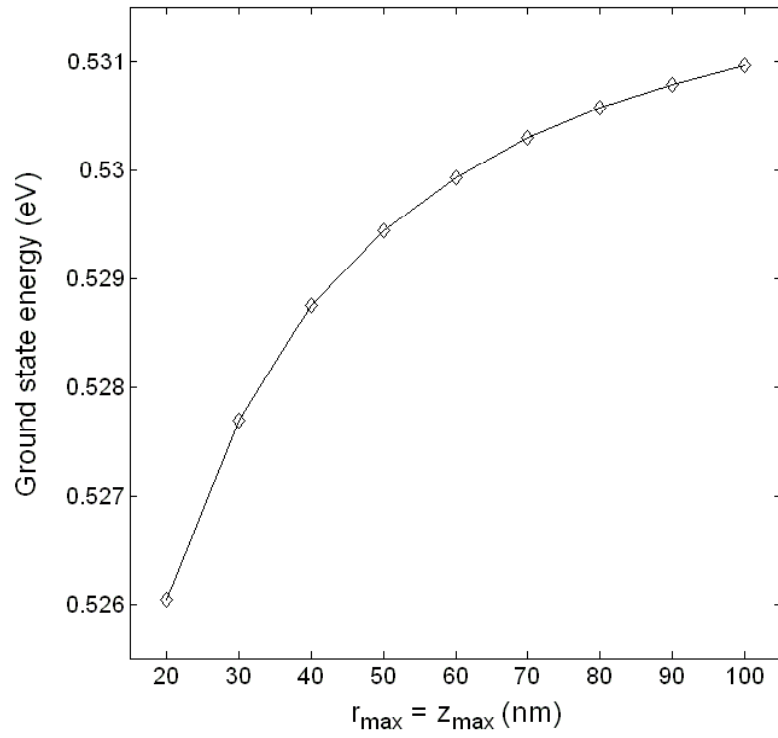


Figure 11.1: The effect of the domain size on the ground state energy of two-electron system with the basis size $N_s = 8$.

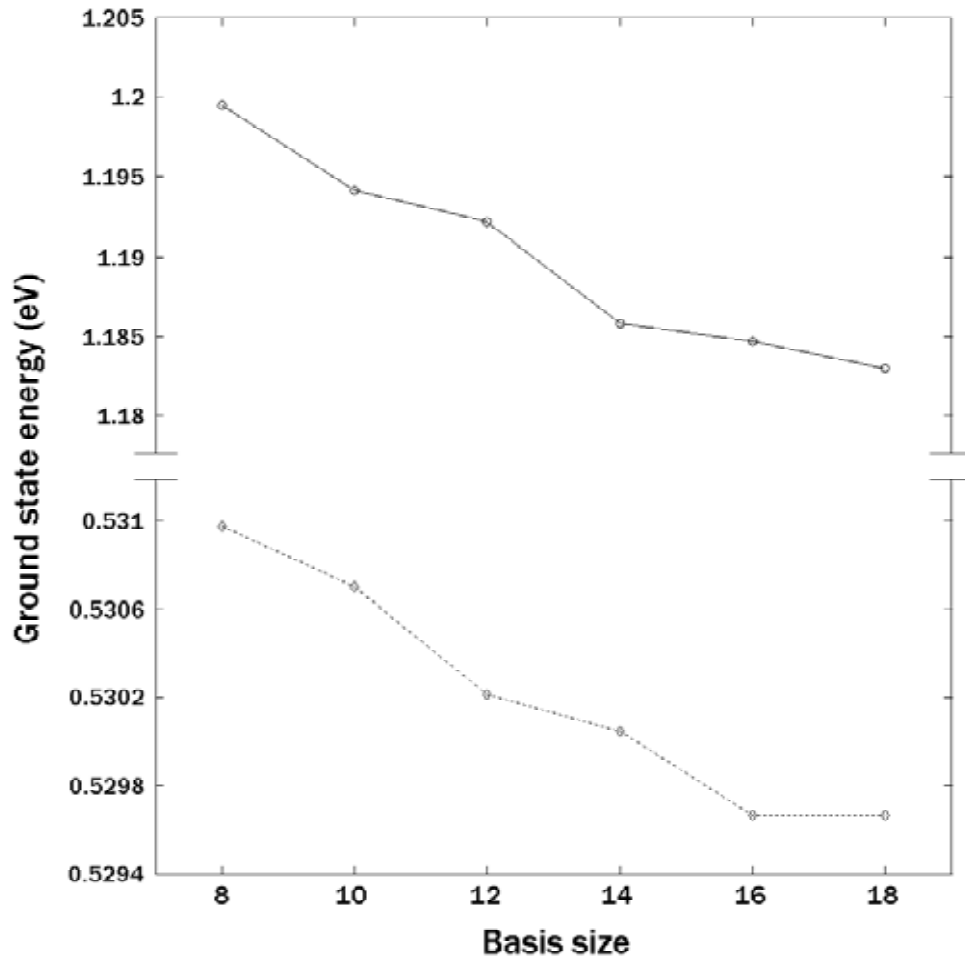


Figure 11.2: The ground state energies of two- and four-electron QDs as a function of the basis size N_s from 8 to 18.

Chapter 12

Concluding Remarks

We have presented a numerical approach to the exact diagonalization of many-electron Hamiltonian in semiconductor quantum dots within the nonparabolic effective mass and realistic 3D confinement potential approximation. The many-electron wave function is expanded in a basis of Slater determinants constructed from numerical wave functions of the single-particle Hamiltonian system. The finite confinement potential implies the boundedness of the single-particle states and thus the finite dimensionality of the function space of many-electron wave functions.

It has been shown that we only need about $N_s = 18$ single-particle states to obtain a convergent ground state energy of a 4-electron system within meV (milli-electron volts) accuracy. The complexity for calculating all pair-wise Coulomb interactions is $O(N_s^2)$. All numerical methods used in our algorithm are stable and convergent. The approach proposed here is whereby robust for more general, realistic, and accurate models of nanoscale semiconductor heterostructures.

Chapter 13

Conclusions

This thesis studies two methods in calculating the electronic energy spectrum of the many-electron Hamiltonian: the current spin density functional theory and the exact diagonalization technique. The main characteristics and results of our models are summarized as follows:

Part I. QDM based on the current spin density functional theory.

- (1) We propose a new mathematical model that incorporates the nonparabolic energy dispersion relation and realistic hard-wall finite confinement potential into the many-body Hamiltonian in the current spin density functional theory in 3D setting.
- (2) A QDM that consists of three vertically aligned semiconductor quantum dots (one large central dot and two smaller identical dots) under the influence of magnetic fields is used in numerical implementation.
- (3) Instead of using deflation scheme in the JD solver [25], a new JD method that allows us to compute several eigenpairs simultaneously and to have a block implementation of the search subspaces is given to solve the cubic

eigenvalue problem resulting from finite difference approximation due to the nonparabolic nature of the effective mass.

- (4) From Tables 3 and 4, the accuracy of the exchange energies is verified by the ratio between the absolute values of $\frac{1}{2} \langle V_H \rangle$ and E_x . This ratio, in accordance with the literature [37] [38], is approximately 2.
- (5) In Fig. 4.2, it is shown that six electrons residing in the large central dot at zero magnetic field can be changed to such that each dot contains two electrons with some feasible magnetic field. The Förster energy transfer may therefore be generated by two individual QDMs. This may motivate a new paradigm of Fermionic qubits for quantum computing in solid-state systems.

Part II. A numerical method for exact diagonalization of semiconductor QD model.



- (1) In this approach, the QD model used is based on realistic 3D finite hard-wall confinement potential and nonparabolic EMA that render analytical basis functions such as Laguerre polynomials inaccessible for the numerical treatment of this kind of models.
- (2) The many-electron wave function is expanded in a basis of Slater determinants constructed from numerical wave functions of the single-electron Hamiltonian with the nonparabolic EMA.

- (3) The cubic eigenvalue problems resulting from the calculations of single-electron basis states are solved by using JD method described as above.
- (4) As shown in Fig. 11.1, the long-range character of the Coulomb interaction has a profound influence on the ground state energy. Thus, the finite difference approximations of the Schrödinger equations and the Poisson equations are performed on a rather large domain with nonuniform mesh.
- (5) From Fig. 11.2, it is evident that a good convergence can be achieved by means of a few single-electron basis states.

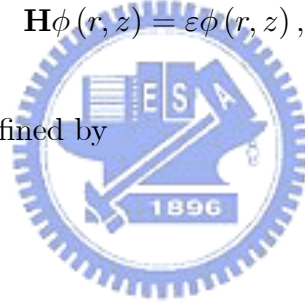


Appendix

In this appendix, a derivation of the resulting cubic eigenvalue problem (3.20) (or(8.7)) from the finite difference discretization is briefly sketched. For simplicity, we only consider the case in which nonlinear terms are neglected, that is

$$\mathbf{H}\phi(r, z) = \varepsilon\phi(r, z), \quad (\text{A.1})$$

where the Hamiltonian is defined by



$$\mathbf{H} = T_S + T_B + V_{ext} + V_B, \quad (\text{A.2})$$

$$T_S(r, z) = -\frac{\hbar^2}{2m(r, z, \varepsilon)} \left(\frac{\partial^2}{\partial r^2} + \frac{1}{r} \frac{\partial}{\partial r} - \frac{l^2}{r^2} + \frac{\partial^2}{\partial z^2} \right), \quad (\text{A.3})$$

$$T_B(r, z) = \frac{e^2 B^2 r^2}{8m(r, z, \varepsilon)} + \frac{\hbar e B l}{2m(r, z, \varepsilon)}, \quad (\text{A.4})$$

$$V_{ext}(r, z) = \begin{cases} 0, & \text{in } \bar{\Omega}_{InAs} \\ V_0, & \text{in } \bar{\Omega}_{GaAs}. \end{cases}, \quad (\text{A.5})$$

$$V_B(r, z) = \sigma \frac{1}{2} g(r, z, \varepsilon) \mu_B B. \quad (\text{A.6})$$

For convenience, we define some notations as follows

$$M_1 \equiv E_g(r, z) - V_{ext}(r, z), \quad (\text{A.7})$$

$$M_2 \equiv E_g(r, z) - V_{ext}(r, z) + \Delta(r, z). \quad (\text{A.8})$$

Then, the effective mass and the Landé factor can be rewritten as

$$\frac{1}{m(r, z, \varepsilon)} = \frac{p^2}{\hbar^2} \left[\frac{3\varepsilon + M_1 + 2M_2}{(\varepsilon + M_1) \times (\varepsilon + M_2)} \right], \quad (\text{A.9})$$

$$g(r, z, \varepsilon) = 2 \left\{ \frac{[\hbar^2 \times (\varepsilon + M_1) \times (\varepsilon + M_2)] - (m_0 p^2 \Delta(r, z))}{\hbar^2 \times (\varepsilon + M_1) \times (\varepsilon + M_2)} \right\}. \quad (\text{A.10})$$

By using the standard central finite difference method and substituting the expressions of the effective mass and the Landé factor into (A.1), we have

$$\begin{aligned} 0 = & -\frac{p^2 (3\varepsilon + M_1 + 2M_2)}{2(\varepsilon + M_1) \times (\varepsilon + M_2)} \left[\frac{\phi_{i,j+1} - 2\phi_{i,j} + \phi_{i,j-1}}{(\Delta r)^2} + \frac{1}{r_j} \frac{\phi_{i,j+1} - \phi_{i,j-1}}{2\Delta r} \right. \\ & \left. - \frac{l^2}{r_j^2} \phi_{i,j} + \frac{\phi_{i+1,j} - 2\phi_{i,j} + \phi_{i-1,j}}{(\Delta z)^2} \right] \\ & + \left\{ \frac{e^2 B^2 r_j^2 p^2 (3\varepsilon + M_1 + 2M_2)}{8\hbar^2 (\varepsilon + M_1) \times (\varepsilon + M_2)} + \frac{\hbar e B l p^2 (3\varepsilon + M_1 + 2M_2)}{2\hbar^2 (\varepsilon + M_1) \times (\varepsilon + M_2)} + V_{ext}(r_j, z_i) \right. \\ & \left. + \sigma \mu_B B \left[\frac{\hbar^2 \times (\varepsilon + M_1) \times (\varepsilon + M_2) - (m_0 p^2 \Delta(r_j, z_i))}{\hbar^2 \times (\varepsilon + M_1) \times (\varepsilon + M_2)} \right] - \varepsilon \right\} \phi_{i,j}. \quad (\text{A.11}) \end{aligned}$$

where Δr and Δz are mesh lengths in r and z directions, respectively, and $\phi_{i,j}$ is an approximated value of function ϕ at the grid point (r_j, z_i) for $i = 1, \dots, n$, and $j = 1, \dots, n$. Here, the index n denotes the grid point number. In Part I, all numerical

results are obtained on the uniform grids, i.e., $\Delta r = \Delta z$. But in Part II, due to the long-range tail of the Coulomb interaction, the large computational domain is required to achieve acceptable accuracy in calculating the ground state energy so that we must use the nonuniform grids. Furthermore, different formulations are instead of the finite difference representations of one- and two-order derivatives. In this appendix, we just give an example of the uniform finite difference scheme.

Finally, by multiplying the common denominator $(\varepsilon + M_1) \times (\varepsilon + M_2)$ to (A.11), we obtain

$$\begin{aligned}
0 = & -\frac{p^2(3\varepsilon + M_1 + 2M_2)}{2} \left[\frac{\phi_{i,j+1} - 2\phi_{i,j} + \phi_{i,j-1}}{(\Delta r)^2} + \frac{1}{r_j} \frac{\phi_{i,j+1} - \phi_{i,j-1}}{2\Delta r} \right. \\
& \left. - \frac{l^2}{r_j^2} \phi_{i,j} + \frac{\phi_{i+1,j} - 2\phi_{i,j} + \phi_{i-1,j}}{(\Delta z)^2} \right] \\
& + \left\{ \frac{e^2 B^2 r_j^2 p^2 (3\varepsilon + M_1 + 2M_2)}{8\hbar^2} + \frac{\hbar e B l p^2 (3\varepsilon + M_1 + 2M_2)}{2\hbar^2} \right. \\
& + V_{ext}(r_j, z_i) \times (\varepsilon + M_1) \times (\varepsilon + M_2) \\
& + \sigma \mu_B B \left[\frac{\hbar^2 \times (\varepsilon + M_1) \times (\varepsilon + M_2) - (m_0 p^2 \Delta(r_j, z_i))}{\hbar^2} \right] \\
& \left. - \varepsilon \times (\varepsilon + M_1) \times (\varepsilon + M_2) \right\} \phi_{i,j}. \tag{A.12}
\end{aligned}$$

Note that same manipulation treatments are used in the discretizations of the interface and the boundary conditions. Thus, the finite difference approach of (A.1) will result in a cubic eigenvalue problem (3.20) (or(8.7)) .

In order to make the problem clear, we classify the matrix coefficients as follows:

Table A1. coefficients of matrix A_3

$$\phi_{i-1,j} \quad 0$$

$$\phi_{i,j-1} \quad 0$$

$$\phi_{i,j} \quad -1$$

$$\phi_{i,j+1} \quad 0$$

$$\phi_{i+1,j} \quad 0$$

Table A2. coefficients of matrix A_2

$$\phi_{i-1,j} \quad 0$$

$$\phi_{i,j-1} \quad 0$$

$$\phi_{i,j} \quad \sigma\mu_B B + V_{ext}(r_j, z_i) - (M_1 + M_2)$$

$$\phi_{i,j+1} \quad 0$$

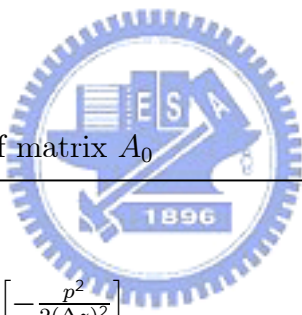
$$\phi_{i+1,j} \quad 0$$



Table A3. coefficients of matrix A_1

$$\begin{aligned}
 \phi_{i-1,j} &= -\frac{3p^2}{2(\Delta z)^2} \\
 \phi_{i,j-1} &= -\frac{3p^2}{2(\Delta r)^2} + \frac{3p^2}{4r_j\Delta r} \\
 \phi_{i,j} &= \frac{3p^2}{(\Delta z)^2} + \frac{3p^2}{(\Delta r)^2} + \frac{3l^2p^2}{2(r_j)^2} + \frac{3e^2B^2(r_j)^2p^2}{8\hbar^2} + \frac{3eBlp^2}{2\hbar} + \sigma\mu_B B(M_1 + M_2) \\
 &\quad + V_{ext}(r_j, z_i)(M_1 + M_2) - M_1M_2 \\
 \phi_{i,j+1} &= -\frac{3p^2}{2(\Delta r)^2} - \frac{3p^2}{4r_j\Delta r} \\
 \phi_{i+1,j} &= -\frac{3p^2}{2(\Delta z)^2}
 \end{aligned}$$

Table A4. coefficients of matrix A_0



$$\begin{aligned}
 \phi_{i-1,j} &= (M_1 + 2M_2) \times \left[-\frac{p^2}{2(\Delta z)^2} \right] \\
 \phi_{i,j-1} &= (M_1 + 2M_2) \times \left[-\frac{p^2}{2(\Delta r)^2} + \frac{p^2}{4r_j\Delta r} \right] \\
 \phi_{i,j} &= (M_1 + 2M_2) \times \left[\frac{p^2}{(\Delta z)^2} + \frac{p^2}{(\Delta r)^2} + \frac{l^2p^2}{2(r_j)^2} + \frac{e^2B^2(r_j)^2p^2}{8\hbar^2} + \frac{eBlp^2}{2\hbar} \right] \\
 &\quad + M_1M_2 \times [\sigma\mu_B B + V_{ext}(r_j, z_i)] - \frac{m_0p^2\Delta(r_j, z_i)\sigma\mu_B B}{\hbar^2} \\
 \phi_{i,j+1} &= (M_1 + 2M_2) \times \left[-\frac{p^2}{2(\Delta r)^2} - \frac{p^2}{4r_j\Delta r} \right] \\
 \phi_{i+1,j} &= (M_1 + 2M_2) \times \left[-\frac{p^2}{2(\Delta z)^2} \right]
 \end{aligned}$$

Bibliography

- [1] D. P. DiVincenzo, Quantum computation, *Science* 270 (1995) 255.
- [2] B. E. Kane, A silicon-based nuclear spin quantum computer, *Nature* 393 (1998) 133.
- [3] A. Imamoglu, D. D. Awschalom, G. Burkard, D. P. DiVincenzo, D. Loss, M. Sherwin, and A. Small, Quantum information processing using quantum dot spins and cavity QED, *Phys. Rev. Lett.* 83 (1999) 4204.
- [4] E. Biolatti, R. C. Iotti, P. Zanardi, and F. Rossi, Quantum information processing with semiconductor macroatoms, *Phys. Rev. Lett.* 85 (2000) 5647.
- [5] P. M. Petroff, A. Lorke, and A. Imamoglu, Epitaxially self-assembled quantum dots, *Physics Today* 54 (2001) 46.
- [6] M. Bayer, P. Hawrylak, K. Hinzer, S. Fafard, M. Korkusinski, Z. R. Wasilewski, O. Stern, and A. Forchel, Coupling and entangling of quantum states in quantum dot molecules, *Science* 291 (2001) 451.
- [7] B. W. Lovett, J. H. Reina, A. Nazir, and G. A. D. Briggs, Optical schemes for quantum computation in quantum dot molecules, *Phys. Rev. B* 68 (2003) 205319.

- [8] J. M. Elzerman, R. Hanson, L. H. Willems van Beveren, B. Witkamp, L. M. K. Vandersypen and L. P. Kouwenhoven, Single-shot read-out of an individual electron spin in a quantum dot, *Nature* 430 (2004) 431.
- [9] G. Ortner, I. Yugova, G. Baldassarri Höger von Högersthal, A. Larionov, H. Kurtze, D. R. Yakovlev, M. Bayer, S. Fafard, Z. Wasilewski, and P. Hawrylak, Y. B. Lyanda-Geller, T. L. Reinecke, A. Babinski, M. Potemski, V. B. Timofeev and A. Forchel, Fine structure in the excitonic emission of InAs/GaAs quantum dot molecules, *Phys. Rev. B* 71 (2005) 125335.
- [10] H.-A. Engel and D. Loss, Fermionic Bell-state analyzer for spin qubits, *Science* 309 (2005) 586.
- [11] S. A. Crooker, J. A. Hollingsworth, S. Tretiak, and V. I. Klimov, Spectrally resolved dynamics of energy transfer in quantum-dot assemblies: towards engineered energy flows in artificial materials, *Phys. Rev. Lett.* 89 (2002) 186802.
- [12] X. Hu, T. Ritz, A. Damjanovic, F. Autenrieth, and K. Schulten, Photosynthetic apparatus of purple bacteria, *Quarterly Rev. of Biophysics*, 35 (2002) 1.
- [13] C. Hettich, C. Schmitt, J. Zitzmann, S. Kuhn, I. Gerhardt, and V. Sandoghdar, Nanometer resolution and coherent optical dipole coupling of two individual molecules, *Science* 298 (2002) 385.
- [14] C. R. Kagn, C. B. Murray, M. Nirmal, and M. G. Bawendi, Electronic energy transfer in CdSe quantum dot solids, *Phys. Rev. Lett.* 76 (1996) 1517.
- [15] G. Vignale and M. Rasolt, Density-functional theory in strong magnetic fields, *Phys. Rev. Lett.* 59 (1987) 2360.
- [16] G. Vignale and M. Rasolt, Current- and spin-density-functional theory for inhomogeneous electronic systems in strong magnetic fields, *Phys. Rev. B* 37 (1988) 10685.

- [17] H. Saarikoski, E. Räsänen, S. Siljämäki, A. Harju, M. J. Puska, and R. M. Nieminen, Testing of two-dimensional local approximations in the current-spin and spin-density-functional theories, *Phys. Rev. B* 67 (2003) 205327.
- [18] E. Räsänen, A. Harju, M. J. Puska, and R. M. Nieminen, Rectangular quantum dots in high magnetic fields, *Phys. Rev. B* 69 (2004) 165309.
- [19] H. Jiang, D. Ullmo, W. Yang, and H. U. Baranger, Electron-electron interactions in isolated and realistic quantum dots: A density functional theory study, *Phys. Rev. B* 69 (2004) 235326.
- [20] E. A. de Andrada e Silva, G. C. La Rocca, and F. Bassani, Spin-split subbands and magneto-oscillations in III-V asymmetric heterostructures, *Phys. Rev. B* 50 (1994) 8523.
- [21] O. Voskoboynikov, C. P. Lee, and O. Tretyak, Spin-orbit splitting in semiconductor quantum dots with a parabolic confinement potential, *Phys. Rev. B* 63 (2001) 165306.
- [22] Y. Li, J.-L. Liu, O. Voskoboynikov, C. P. Lee, and S. M. Sze, Electron energy level calculations for cylindrical narrow gap semiconductor quantum dot, *Comput. Phys. Commun.* 140 (2001) 399-404.
- [23] J. I. Climente, J. Planelles, and J. L. Movilla, Magnetization of nanoscopic quantum rings and dots, *Phys. Rev. B* 70 (2004) 081301.
- [24] W. Wang, T.-M. Hwang, W.-W. Lin, and J.-L. Liu, Numerical methods for semiconductor heterostructures with band nonparabolicity, *J. Comp. Phys.* 189 (2003) 579-606.
- [25] T.-M. Hwang, W.-W. Lin, J.-L. Liu, W. Wang, Jacobi-Davidson methods for cubic eigenvalue problems, *Num. Lin. Alg. Appl.* 12 (2005) 605-624.

- [26] P. Hohenberg and W. Kohn, Inhomogeneous electron gas, *Phys. Rev.* 136 (1964) B864.
- [27] W. Kohn and L. J. Sham, Self consistent equations including exchange and correlation effects, *Phys. Rev.* 140 (1965) A1133.
- [28] S. M. Reimann and M. Manninen, Electronic structure of quantum dots, *Rev. Mod. Phys.* 74 (2002) 1283-1342.
- [29] Y. Li, O. Voskoboynikov, C. P. Lee and S. M. Sze, Energy and coordinate dependent effective mass and confined electron states in quantum dots, *Solid State Comm.* 120 (2001) 79.
- [30] G. Vignale, M. Rasolt, and D. J. W. Geldart, Diamagnetic susceptibility of a dense electron gas, *Phys. Rev. B* **37**, 2502 (1988).
- [31] J. P. Perdew and Y. Wang, Accurate and simple analytic representation of the electron-gas correlation energy, *Phys. Rev. B* 45 (1992) 13244.
- [32] T. L. Beck, Real-space mesh techniques in density-functional theory, *Rev. Mod. Phys.* 72 (2000) 1041.
- [33] A. Stathopoulos, S. Ögüt, Y. Saad, J. Chelikowsky, H. Kim, Parallel methods and tools for predicting material properties, *Comput. Sci. Engrg.* 3 (2000) 19.
- [34] R. Barrett, M. Berry, T. F. Chan, J. Demmel, J. Donato, J. Dongarra, V. Eijkhout, R. Pozo, C. Romine, and H. Van der Vorst, *Templates for the Solution of Linear Systems: Building Blocks for Iterative Methods*, 2nd Ed., SIAM, Philadelphia (1994).
- [35] M. Crouzeix, B. Philippe, and M. Sadkane, The Davidson method, *SIAM J. Sci. Comput.* 15 (1994) 62.

- [36] G. Golub and C. van Loan, Matrix Computations, 3rd ed., The Johns Hopkins University Press (1996).
- [37] C.-J. Huang and C. J. Umrigar, Local correlation energies of two-electron atoms and model systems, Phys. Rev. A 56 (1997) 290.
- [38] C. Filippi, C. J. Umrigar, and M. Taut, Comparison of exact and approximate density functionals for an exactly soluble model, J. Chem. Phys. 100 (1994) 1290-1296.
- [39] A. Alavi, Two interacting electrons in a box: An exact diagonalization study, J. Chem. Phys. 113 (2000) 7735-7745.
- [40] Z. Bai, J. Demmel, J. Dongarra, A. Ruhe, H. van der Vorst (Eds.), Templates for the Solution of Algebraic Eigenvalue Problems: A Practical Guide, SIAM, Philadelphia, 2000.
- [41] J. A. Barker, R. J. Warburton, and E. P. O'Reilly, Electron and hole wave functions in self-assembled quantum rings, Phys. Rev. B 69 (2004) 035327.
- [42] D. Bellucci, M. Rontani, F. Troiani, G. Goldoni, and E. Molinari, Competing mechanisms for singlet-triplet transition in artificial molecules, Phys. Rev. B 69 (2004) 201308.
- [43] N. A. Bruce and P. A. Maksym, Quantum states of interacting electrons in a real quantum dot, Phys. Rev. B 61 (2000) 4718-4726.
- [44] T. Chakraborty and P. Pietiläinen, Optical signatures of spin-orbit interaction effects in a parabolic quantum dot, Phys. Rev. Lett. 95 (2005) 136603.
- [45] I. Filikhin, V. M. Suslov, and B. Vlahovic, Modeling of InAs/GaAs quantum ring capacitance spectroscopy in the nonparabolic approximation, Phys. Rev. B 73 (2006) 205332.

- [46] C. P. Garcia, V. Pellegrini, A. Pinczuk, M. Rontani, G. Goldoni, E. Molinari, B. S. Dennis, L. N. Pfeiffer, and K. W. West, Evidence of correlation in spin excitations of few-electron quantum dots, *Phys. Rev. Lett.* 95 (2005) 266806.
- [47] M. Korkusinski, P. Hawrylak, M. Ciorga, M. Pioro-Ladriere, and A. S. Sachrajda, Pairing of spin excitations in lateral quantum dots, *Phys. Rev. Lett.* 93 (2004) 206806.
- [48] J. C. Lin and G. Y. Guo, Current-spin density-functional theory of the electronic and magnetic properties of quantum dots and quantum rings, *Phys. Rev. B* 65 (2002) 035304.
- [49] J.-L. Liu, J.-H. Chen, and O. Voskoboynikov, A model for semiconductor quantum dot molecule based on the current spin density functional theory, *Comput. Phys. Commun.* 175 (2006) 575-582.
- [50] P. Lucignano, B. Jouault, and A. Tagliacozzo, Spin exciton in a quantum dot with spin-orbit coupling at high magnetic field, *Phys. Rev. B* 69 (2004) 045314.
- [51] P. A. Maksym and T. Chakraborty, Quantum dots in a magnetic field: Role of electron-electron interactions, *Phys. Rev. Lett.* 65 (1990) 108-111.
- [52] D. Pfannkuche and V. Gudmundsson, Comparison of a Hartree, a Hartree-Fock, and an exact treatment of quantum-dot helium, *Phys. Rev. B* 47 (1993) 2244-2250.
- [53] P. Pietiläinen and T. Chakraborty, Energy levels and magneto-optical transitions in parabolic quantum dots with spin-orbit coupling, *Phys. Rev. B* 73 (2006) 155315.
- [54] M. Rontani, F. Rossi, F. Manghi, and E. Molinari, Coulomb correlation effects in semiconductor quantum dots: The role of dimensionality, *Phys. Rev. B* 59 (1999) 10165-10175.

- [55] M. Roy and P. A. Maksym, Efficient method for calculating electronic states in self-assembled quantum dots, *Phys. Rev. B* 68 (2003) 235308.
- [56] G. L. Sleijpen, A. G. Booten, D. R Fokkema, H. A. van der Vorst, Jacobi-Davidson type methods for generalized eigenproblems and polynomial eigenproblems, *BIT* 36 (1996) 595-633.
- [57] M. C. Strain , G. E. Scuseria and M. J. Frisch, Achieving linear scaling for the electronic quantum Coulomb problem, *Science*, 271 (1996) 51-53.
- [58] M. B. Tavernier, E. Anisimovas, F. M. Peeters, B. Szafran, J. Adamowski, and S. Bednarek, Four-electron quantum dot in a magnetic field, *Phys. Rev. B* 68 (2003) 205305.
- [59] H. Voss, Iterative projection methods for computing relevant energy states of a quantum dot, *J. Comp. Phys.* 217 (2006) 824-833.
- [60] O. Voskoboynikov, Y. Li, H.-M. Lu, C.-F. Shih, and C. P. Lee, Energy states and magnetization in nanoscale quantum rings, *Phys. Rev. B* 66 (2002) 155306.
- [61] A. Wojs, P. Hawrylak, S. Fafard, and L. Jacak, Electronic structure and magneto-optics of self-assembled quantum dots, *Phys. Rev. B* 54 (1996) 5604-5608.
- [62] S.-R. E. Yang, A. H. MacDonald, and M. D. Johnson, Addition spectra of quantum dots in strong magnetic fields, *Phys. Rev. Lett.* 71 (1993) 3194-3197.